Modeling the Cloud Curves and the Solubility of Gases in Amorphous and Semicrystalline Polyethylene with the SAFT-VR Approach and Flory Theory of Crystallization

ARTICLE *in* INDUSTRIAL & ENGINEERING CHEMISTRY RESEARCH · SEPTEMBER 2004

Impact Factor: 2.59 · DOI: 10.1021/ie049592a

3 AUTHORS, INCLUDING:

Patrice Paricaud
ENSTA-ParisTech, Université Paris-Saclay
42 PUBLICATIONS **821** CITATIONS
SEE PROFILE

Amparo Galindo
Imperial College London
117 PUBLICATIONS **3,880** CITATIONS
SEE PROFILE

Modeling the Cloud Curves and the Solubility of Gases in Amorphous and Semicrystalline Polyethylene with the SAFT-VR Approach and Flory Theory of Crystallization

Patrice Paricaud,[†] Amparo Galindo,[‡] and George Jackson*[,‡]

Department of Chemical Engineering, Vanderbilt University, VU Station B, Box 351604, Nashville, Tennessee 37235-1604, and Department of Chemical Engineering and Chemical Technology, Imperial College London, South Kensington Campus, London SW7 2AZ, UK

The statistical associating fluid theory for potentials of variable range SAFT-VR [Gil-Villegas, A.; et al. *J. Chem. Phys.* **1997**, *106*, 4168] is used to examine the fluid-phase behavior of mixtures of *n*-alkanes, alk-1-enes (α-olefins), and nitrogen with polyethylene. The molecules are modeled as flexible chains of tangent spherical segments, with segment−segment dispersive interactions treated via square-well potentials. The parameters of the polyethylene polymer are determined from those of the *n*-alkanes by using simple extrapolations with molecular weight. As a test of the extrapolated parameters for polyethylene, the absorption (vapor−liquid equilibria) and cloud curves (liquid−liquid equilibria) of *n*-pentane−polyethylene systems are predicted without adjustable binary parameters, and the effect of the polymer parameters on the phase behavior of the mixture is discussed. The liquid−liquid immiscibility curve is found to be very sensitive to the intermolecular potential parameters used to describe the polymer. The change in the lower critical solution temperature (LCST) for mixtures of *n*-alkanes of increasing chain length in polyethylene is also predicted. Good agreement with experimental data is also obtained for the absorption of small gases in amorphous polyethylene. The predictions of the SAFT-VR approach confirm experimental findings that the solubility of nitrogen increases with temperature while the solubility of heavier molecules such as ethene and but-1-ene decreases. Strong synergies can be observed when several gases absorb in the same polyethylene polymer. The co-absorption effects are explained in terms of the interactions between gas and polyethylene molecules. When the temperature of interest is below the melting temperature of polyethylene, the polymer exists in a semicrystalline state. In this case, the crystallinity of polyethylene has to be taken into account in order to predict the solubility of the various gases. We present an accurate theory to predict the crystallinity of polyethylene as a function of temperature. The approach, which is based on Flory's theory of copolymer crystallinity [Flory, P. J. *Trans. Faraday Soc.* **1955**, *51*, 848], is accurate for a large variety of polyethylene samples, and requires only the experimental crystallinity or polymer density at 25 °C as an input parameter. On combining the Flory and SAFT-VR approaches, we can predict the solubility of various gases in semicrystalline polyethylene samples, by assuming that the molecules of gas only absorb in the amorphous regions of the polymer.

1. Introduction

An accurate understanding of the phase behavior of polymer−solvent systems is of crucial practical importance in polymer production and processing. During a gas-phase polymerization reaction, polymer particles are suspended by a gas flow and the monomers must sorb into the polymer sample and diffuse through the grain to reach the catalytic sites.[1] The rate of the reaction depends directly on the solubility of the monomer at the active site. It is also important to have a knowledge of the solubility of gases in the polymer to eliminate as much as possible of the absorbed gases from the polymer for reasons of safety and economics:[2] fires have occurred in numerous polymer production plants due to the absorbed flammable gas in the polymer;[3,4] it is also good practice to recycle as much as of the unreacted monomer gas as possible. Polymer−solvent systems exhibit a rich phase behavior with regions of vapor−liquid equilibria (VLE), and liquid−liquid equilibria (LLE) with upper and/or lower critical solution temperatures. Using the thermodynamic perturbation theory (TPT1) of Wertheim,[5−8] we have recently discussed the thermodynamic basis for the liquid−liquid demixing seen in systems which exhibit lower critical solution temperatures (LCSTs).[9] In particular, we have shown that in polymer solutions this type of demixing is principally due to contraction effects, which induce a negative entropy of mixing leading to phase separation. This liquid−liquid equilibria is due to entirely different effects than the phase separation observed in polymer−colloid systems, which is driven by a large unfavorable enthalpic contribution induced by the colloid−polymer excluded volume interactions.[10]

In this paper we focus on the regions of vapor−liquid equilibria in which the solvent behaves as an absorbed gas in the polymer. At temperatures below the melting point of the polymer, amorphous and crystalline regions

* To whom correspondence should be addressed. E-mail: g.jackson@imperial.ac.uk.
[†] Vanderbilt University.
[‡] Imperial College London.

10.1021/ie049592a CCC: $27.50
Published on Web 09/17/2004

are observed in the sample, and the solid phases have to be taken into account. The sorption of gases in a polymer is a bulk process, as the gas molecules can usually diffuse through the amorphous parts of the polymer sample, and the terms "absorption" or "solubility" are more appropriate than the term "adsorption," which usually refers to a surface process. The crystalline parts of the polymer, also called "crystallites", behave as a barrier against the diffusion of the gas molecules in the sample. As a result, it is usually assumed that the gas molecules cannot penetrate the crystallites for steric reasons and only absorb in the amorphous regions.[2,11−14] A thermodynamic consideration of fluid−solid equilibria supports this assumption as the proportion of a solvent in the coexisting solid phase is invariably very low. When the polymer is semicrystalline, the amorphous regions present a liquidlike structure and one can apply a theory for fluid phases to describe the thermodynamic properties of the amorphous phase. The absorption of gases in polyethylene can thus be modeled as a vapor−liquid equilibrium between a gas phase where no polymer molecules are present, and a liquid phase consisting of gas molecules absorbing into an amorphous polymer matrix.[11]

Over the past sixty years numerous theories have been used to describe the fluid-phase equilibria of polymer systems (an excellent review can be found in reference 15; see reference 9 for a recent update). Three types of approaches have been considered in modeling the vapor−liquid equilibria of polymer systems: activity coefficient approaches, lattice models, and equations of state. Activity coefficient approaches include the UNIFAC-free volume (UNIFAC-FV) model of Oishi and Prausnitz,[16] the entropic-FV model of Elbro et al.,[17] the GK-FV model of Kontogeorgis et al.,[18] the UNIFAC-ZM model of Zhong et al.,[19] and the polymer-NRTL method.[20] Details of these can be found in references 15 and 21. These models accurately describe the activity coefficient of gases in polymer for a large variety of binary mixtures,[21] and can be used to model both vapor−liquid and liquid−liquid-phase equilibria. However, they require the use of temperature-dependent binary parameters if they are to be applied over a wide range of conditions. An additional problem with activity coefficient models is that they cannot be used to represent pressure effects accurately, and hence are not suited to studies of liquid−liquid equilibria with LCSTs.

The vast majority of lattice models developed to describe the fluid-phase equilibria in polymeric systems are based on the well-known Flory−Huggins−Staverman theory.[22−24] One of the most widely used is the Sanchez−Lacombe[25,26] equation of state, which essentially describes a compressible version of the Flory−Huggins lattice model where volume effects are incorporated via vacant lattice sites. For applications of the Sanchez−Lacombe equation and other lattice models to real systems, the reader is directed to the reviews in refs 15, 27, and 28. It should be noted that, as in the case of activity coefficient approaches, state-dependent binary interaction parameters are usually required to describe the phase equilibria over wide ranges of temperature, pressure, and composition with the lattice approaches.[29−31] A recent lattice approach based on the Born−Yvon−Green (BYG) integral equation theory,[32−35] which includes an explicit treatment of the correlations between the segments, has been successfully applied to polymer solutions and blends. Luettmer-Strathmann and Lipson[36] have used this BYG lattice description to examine fluid-phase separation and LCSTs in mixtures of alkanes and polyethylene, describing the experimental phase behavior accurately without the need for adjustable or state-dependent binary parameters.

The third class of approaches for polymeric molecules are those based on equations of state (EOS) which treat the fluid phase as a continuum. The advantage of EOS approaches with respect to the other approaches is that they can be applied over wide ranges of temperature and pressure. A number of equations of state have been used in engineering applications to describe the vapor−liquid and liquid−liquid immiscibility in polymer systems; one such example is the combination of the Soave−Redlich−Kwong EOS with the Flory−Huggins−Staverman lattice theory.[37,38] An alternative continuum approach for chain molecules was developed by Wertheim[39] by examining the free energy of an equivalent associating fluid. Wertheim used a first-order thermodynamic perturbation theory (TPT1) to determine the thermodynamic properties of associating fluids.[5−8] In the limit of infinitely strong association a simple expression is obtained for the EOS of a fully flexible chain fluid.[39,40] This approach is at the core of the development of equations of state for chain molecules formed from spherical segments, such as the statistical associating fluid theory (SAFT)[41−44] in its numerous incarnations. The reader can find a comprehensive list of the most recent applications of the SAFT EOS to real systems in the reviews of Müller and Gubbins.[45,46]

The most recent versions of the SAFT EOS include the soft-SAFT,[47,48] the variable-range SAFT-VR,[49,50] and the perturbed-chain PC-SAFT[51,52] descriptions. The differences among these arise from the specific treatment of the attractive intersegment interactions and the choice of reference fluid. The soft-SAFT approach is based on segments interacting through a Lennard−Jones potential (see ref 53), with a hard-sphere fluid as the reference in the perturbation theory. In addition a very accurate dimer version of the approach has been developed[54] (also see ref 55), which improves the description of the fluid-phase equilibria for longer chains. In the case of the PC-SAFT EOS, a hard-sphere chain fluid is used as the reference instead of a hard-sphere fluid. The attractive term of the PC-SAFT equation, which was originally based on that of a Lennard−Jones system, was empirically modified to fit the experimental vapor pressures and saturated densities of the *n*-alkanes;[51] this modification leads to an excellent description of the thermodyamics of chain molecules. The SAFT-VR equation of state describes fluid of associating chain molecules with the segments of the chain interacting through attractive interactions of variable range (square-well, Sutherland, Yukawa, and Lennard−Jones potentials have all been examined); a reference system of attracting monomers is then used to build up the chain and the associative contributions to the free energy following the TPT1 theory of Wertheim. The main advantage of the SAFT-VR description is that one explicitly includes the range of the intermolecular potential, which allows for the nonconformal nature of the interactions between molecules to be taken into account. The variable range is particularly useful in describing polar molecules such as refrigerants or polyelectrolytes. The interfacial properties are also very sensitive to the range of the potential, imparting a particular advantage to theories which explicitly incor-

porate the range. In this paper, we use the SAFT-VR equation to predict the solubility of gases in polyethylene, closely following the procedure presented in earlier work.[56]

To quantify the total absorption of a gas in a polymer, a knowledge of the crystallinity of the polymer sample as a function of temperature is required. A clear introduction to polymer crystallization can be found in the texts by Mandelkern[57] and by Sharples.[58] Experimental studies on polymer crystallization are very numerous; the reader can find some recent experimental studies on high-density (HDPE) and low-density (LDPE) polyethylene and poly(ethylene-olefins) (or linear low-density polyethylene, LLDPE) crystallization in references 12 and 59−63. In the context of our current study with the SAFT approach it is also important to mention theories which have been used to describe the melting point of model chain molecules. Vega and MacDowell[64] have proposed an extension of the Wertheim TPT1 approach to study the fluid−solid transition of chain molecules. The approach was originally proposed for freely jointed hard-spherical segments, but it has since been shown to be applicable to chains of tangent hard disks,[65] fully flexible hard-chain molecules interacting via mean-field dispersion interactions,[66] and Lennard−Jones chains.[67,68] In the case of the Lennard−Jones systems the global (solid−liquid−vapor) phase behavior has been obtained and compared with computer simulations; the predictions of the approach are in excellent agreement with the exact simulation data.[68] This type of approach would thus appear to be an ideal option for predictions of the boundary of solid−fluid behavior of long chain molecules such as polymers. Unfortunately, the theory of Vega and co-workers is at this stage limited to pure components which crystallize completely into a single solid phase. The melting behavior of polyethylene is more complicated, as the polymer sample is usually a highly polydisperse mixture and does not crystallize completely. Theoretical studies of the melting behavior of polyethylene are very rare, and most of the approaches to predict the crystallinity are empirical. It is very difficult to predict with accuracy the fusion properties of polymers which depend on many different properties that are not often available, including the comonomer composition, the molecular and isomeric structure, the branching, the polydispersity, the lamellar thickness, and the thermal history of the sample.

To our knowledge, the only available theory which provides a good description of the melting behavior of polymers was derived almost fifty years ago by Flory,[69] who proposed an analytical expression for the melting point and the crystallinity of an ideal copolymer. Though it provides an excellent qualitative description of the evolution of the crystallinity of polymers with temperature, Flory's theory has not been applied frequently. Sanchez and Eby[70] have improved Flory's expression for the melting points of copolymers by introducing some extra parameters to take into account defects such as branching, and chain ends. More recently, Kim et al.[71] have tested the adequacy of the Flory[69] and the Sanchez and Eby[70] expressions in predictions of the melting points of LLDPE samples. They conclude that the Sanchez and Eby[70] theory can provide a better description than the Flory theory when the parameters which characterize the defects are refined by using experimental data. Their study is, however, restricted to a specific LLDPE: (poly(ethylene-octene)). Crist and Howard[72] have also assessed the adequacy of the Flory approach for both the melting point and crystallinity data of poly(ethylene-butene) samples, and concluded that the theory overestimates the crystallinity. This overestimation can be explained as follows: in practice, the semicrystalline polymer sample is in a metastable state and the crystallinity depends on the cooling rate; in the simple theory developed by Flory, the crystallinity is determined "at equilibrium" by assuming an infinitely slow cooling rate. In this paper, we present a semiempirical approach based on the Flory theory of polymer crystallization. Our aim is to develop an approach which requires the minimum amount of information about the polymer sample, and overcomes the problem of the thermal history. The idea is to use the Flory expressions to obtain a good qualitative description of the temperature dependence of the crystallinity, and to scale the description to one experimental value in order to obtain a good quantitative prediction over the entire range of temperatures.

The absorption of gases in a semicrystalline polymer is a complex three-phase equilibria between vapor, liquid, and solid phases, and one must be careful of the validity of the hypotheses that are made. The assumption that gas molecules absorb only in the amorphous regions may be too crude: if the gas molecules are very small, such as H_2,[73] they may penetrate into the crystalline lattice and the solubility of gases in the crystallites will not be negligible. Furthermore, the presence of gas molecules in the polymer sample decreases the melting point and the crystallinity of the pure polymer due to cryoscopic effects.[74−76] As a consequence of both of these effects our assumptions could lead to an underestimate of the total absorption. The opposite effect can be observed due to the swelling of the polymer sample after the absorption of a gas: the crystalline zones link the chain molecules together to form a polymer network,[77,78] and when the gas absorbs into the sample, elastic forces opposed to swelling are induced and the system behaves like a polymer gel. In this case the solubility of the gas would be lower than that in the corresponding completely amorphous sample where the polymer molecules are free to expand, and we would overestimate the total absorption. There are clearly a number of important questions: What is the adequacy of our assumptions? Do the induced errors cancel each other? Does one effect dominate the other under different conditions? In this paper we will neglect these effects, and try to answer some of these questions by comparing the predictions with experimental data.

In the last part of our paper we consider systems involving two gases and a polymer. Most of the experimental and theoretical studies of the solubility of gases in polymers are limited to the absorption of a single gas. In practice, however, many different components are present in a gas-phase reactor and simultaneously absorb in the polymer. The solubility of the gases at given partial pressures is usually nonadditive, and a simple Henry's law treatment cannot be applied. It has been observed experimentally[2,79] that the solubility of a gas in a polymer sample may or may not be enhanced by the presence of another gas depending on the nature of this second gas. For instance, the solubility of methane in polyethylene at a fixed partial pressure of methane is enhanced by the presence of ethylene, while the solubility of methane does not change in the presence of nitrogen.[79] The co-absorption problem is an

important industrial issue: in the case of the polymerization of ethylene and α-olefins to make LLDPE, the reaction rate and the final stucture of the polymer chains are directly related to the solubilities of the comonomers in the polyethylene grains. Nath and coworkers[13,80] have recently observed co-absorption effects by Monte Carlo simulation confirming the experimental findings. Co-absorption of two short-chain hydrocarbons (methane, butane, and pentane) in LDPE has also been examined with the SAFT-VR approach.[56] However, the causes of the co-absorption synergy remain unclear. Here, we provide an explanation of these effects following simple thermodynamic arguments by discussing the interactions between the molecules.

This paper is organized as follows: In the next section, the main expressions of the SAFT-VR theory are presented. We then use the SAFT-VR equation to predict the phase behavior of hydrocarbons and polyethylene mixtures, testing the capability of the theory to predict the vapor−liquid and liquid−liquid-phase equilibria. A semiempirical model is then developed based on Flory's theory to predict the crystallinity of polyethylene. Combining our model for crystallinity with the SAFT-VR theory, we predict the solubility of small gases and hydrocarbons in polyethylene. We then discuss the validity of our hypotheses and the co-absorption effects.

2. Fluid-Phase Equilibria with SAFT-VR

In this work all of the fluid phases will be described using the SAFT-VR free energy.[49,50] The amorphous regions of the polymer sample correspond to liquidlike states and can be described with a fluid-phase EOS such as SAFT. In the SAFT-VR approach the molecules are modeled as flexible chains formed from m tangent spherical segments. Each segment in a chain has the same diameter σ, but segments belonging to different species can have different diameters. The dispersive interactions between the segments are modeled via square-well potentials of depth ϵ and variable range λ. Though the form of the potential is rather unrealistic, it facilitates the description of the free energy contributions, while still providing a very good description of the fluid-phase equilibria. The principal expressions of the SAFT-VR equation of state for mixtures with the square-well potential are summarized here; the reader can find the full details in references 49 and 50. In the case of mixtures of chain molecules composed of hard-sphere segments with attractive interactions and associating sites, the Helmholtz free energy can be written as four separate contributions:

$$\frac{A}{NkT} = \frac{A^{IDEAL}}{NkT} + \frac{A^{MONO}}{NkT} + \frac{A^{CHAIN}}{NkT} + \frac{A^{ASSOC}}{NkT} \quad (1)$$

where N is the number of molecules, T is the temperature, and k is the Boltzmann constant. A^{IDEAL} is the free energy of a mixture of ideal gas molecules, A^{MONO} is the contribution due to the interactions between segments, A^{CHAIN} is the contribution due to the formation of chains of segments, and A^{ASSOC} is the contribution due to site−site associations. Note that the latter association term A^{ASSOC} (which is described using the Wertheim TPT1) is not required in the description of systems comprising hydrocarbons and polyethylene as these molecules only interact through van der Waals dispersive forces. The monomer free energy A^{MONO} is obtained from the high-temperature perturbation theory of Barker and Henderson[81−83] with a hard-sphere fluid as the reference system:

$$A^{MONO} = A^{HS} + A_1 + A_2 \quad (2)$$

In this case the repulsive reference free energy A^{HS} is that of a multicomponent mixture of hard spheres described by Boublık[84] and by Mansoori et al.[85] as a generalization of the Carnahan and Starling[86] hard-sphere expression. The attractive terms A_1 and A_2 are obtained by using the Barker and Henderson perturbation theory[81] and the van der Waals (one-fluid) mixing rule (see refs 49 and 50 for the actual expressions). Finally, the contribution to the free energy A^{CHAIN} due to the formation of mixtures of chain molecules of m_i segments is expressed as

$$\frac{A^{CHAIN}}{NkT} = -\sum_i x_i (m_i - 1)\ln g_{ii}^{SW}(\sigma_{ii})) \quad (3)$$

where x_i is the mole fraction of species i, and $g_{ii}^{SW}(\sigma_{ii})$ is the contact value of the pair distribution function of the nonbonded monomers of species i in the mixture; $g^{SW}(\sigma_{ii})$ is derived in terms of a first-order high-temperature expansion as[49,50]

$$g_{ii}^{SW}(\sigma_{ii}) = g_{ii}^{HS}(\sigma_{ii}) + \frac{\epsilon_{ii}}{kT} g_{ii}^{1}(\sigma_{ii}) \quad (4)$$

where $g_{ii}^{HS}(\sigma_{ii})$ is the contact value of the pair distribution function of the hard spheres of species i, and the perturbation term $g_{ii}^{1}(\sigma_{ii})$ is obtained by requiring a self-consistency between the pressure equation (Clausius theorem[87]) and the density derivative of the Helmholtz free energy. In the case of mixtures, the usual combining rules can be used to evaluate the unlike size σ_{ij} and energy ϵ_{ij} interaction parameters:

$$\sigma_{ij} = \frac{\sigma_{ii} + \sigma_{jj}}{2} \quad (5)$$

$$\epsilon_{ij} = (1 - k_{ij})\sqrt{\epsilon_{ii}\epsilon_{jj}} \quad (6)$$

where k_{ij} is a binary parameter which can be adjusted to reproduce the experimental data of binary mixtures. In this study we set k_{ij} to zero (corresponding to the Lorentz−Berthelot combining rule) for the interactions between polyethylene, n-alkanes, and the higher α-olefins. For the interactions between nitrogen or ethylene and polyethylene, only one value for k_{ij} is used for the entire range of temperature and pressure. A simple arithmetic combining rule is used for the range parameter λ_{ij} for the cross interaction square-well potential:

$$\lambda_{ij} = \frac{\lambda_{ii}\sigma_{ii} + \lambda_{jj}\sigma_{jj}}{\sigma_{ii} + \sigma_{jj}} \quad (7)$$

2.1 Pure Components: Alkanes, Olefins, and Polyethylene. Following earlier work,[49,88] we have determined the SAFT-VR intermolecular potential parameters for the n-alkanes up to C_{28} by optimizing the description of the experimental saturated liquid densities and vapor pressures.[89] Here we use a robust annealing optimization method.[90] The same procedure has also been used to determine the intermolecular

Table 1. SAFT-VR Square-Well Parameters for the *n*-alkanes, Ethylene, N_2, and α-Olefins Obtained after Optimization[a]

compound	MW/ (g mol^{-1})	m	λ	σ (Å)	ϵ/k (K)
CH_4	16.04	1	1.4479	3.6847	167.30
C_2H_6	30.07	1.3333	1.4233	3.8115	249.19
C_3H_8	44.10	1.6667	1.4537	3.8899	260.91
C_4H_{10}	58.12	2	1.4922	3.9332	259.56
C_5H_{12}	72.15	2.3333	1.5060	3.9430	264.37
C_6H_{14}	86.18	2.6667	1.5492	3.9396	251.66
C_7H_{16}	100.20	3	1.5574	3.9567	253.28
C_8H_{18}	114.23	3.3333	1.5751	3.9455	249.52
C_9H_{20}	128.26	3.6667	1.5745	3.9635	251.53
$C_{10}H_{22}$	142.28	4	1.5925	3.9675	247.08
$C_{11}H_{24}$	156.31	4.3333	1.5854	3.9775	252.65
$C_{12}H_{26}$	170.33	4.6667	1.6101	3.9663	243.03
$C_{13}H_{28}$	184.36	5	1.6479	3.9583	227.31
$C_{14}H_{30}$	198.39	5.3333	1.6023	3.9745	249.74
$C_{15}H_{32}$	212.41	5.6667	1.5978	3.9964	252.87
$C_{16}H_{34}$	226.44	6	1.6325	3.9810	237.33
$C_{17}H_{36}$	240.47	6.3333	1.6091	3.9954	249.76
$C_{18}H_{38}$	254.49	6.6667	1.6565	3.9562	228.81
$C_{19}H_{40}$	268.52	7	1.6625	3.9713	226.31
$C_{20}H_{42}$	282.55	7.3333	1.6637	3.9726	227.07
$C_{24}H_{50}$	338.65	8.6667	1.6819	3.9809	220.00
$C_{28}H_{58}$	394.76	10	1.6542	3.9896	233.50
PE	MW	0.02376MW	1.6940	4.0100	230.04
N_2	28.01	1.300	1.5340	3.1940	84.53
ethylene	28.05	1.333	1.4432	3.6627	222.17
propene	42.08	1.667	1.4465	3.7839	259.80
but-1-ene	56.11	2.000	1.5564	3.7706	228.49
hex-1-ene	84.16	2.667	1.6244	3.8259	217.78

[a] m corresponds to the number of spherical segments in the model, λ is the range of the square-well potential, σ is the hard-core diameter of each segment, and ϵ is the well depth of the square-well potential.

parameters of ethylene, the higher α-olefins, and nitrogen. All of the parameters are summarized in Table 1. Excellent agreement is obtained with both experimental densities and vapor pressures. As an example, the vapor pressures and coexistence densities of the α-olefins examined in this paper are presented in Figure 1. The description of the fluid-phase behavior for the *n*-alkanes, obtained with parameters very similar to those given in Table 1, was presented in refs 49 and 88. We use the simple empirical relationship $m = (C - 1)/3 + 1$ between the number of carbon atoms C and the number of spherical segments m making up the chain; this provides an excellent representation of the vapor−liquid phase equilibria and bounds the length of the molecule to physically reasonable values.[88]

Linear polyethylene is essentially a very long *n*-alkane and can be modeled as a flexible chain of m spherical segments of the same diameter σ. Following the procedure described in previous work,[88] we represent the SAFT-VR parameters for the long *n*-alkanes and polyethylene using simple linear relations with the molecular weight. The parameters of Table 1 are found to be very similar to those obtained previously,[49,88] and consequently any correlation will also be very similar. Though small variations in the values of the parameters used to describe the longer alkanes and polyethylene do not make a significant difference in studies of absorption (vapor−liquid equilibria) the effect on liquid−liquid equilibria can be dramatic. As we show later in this paper, the calculated liquid−liquid coexistence (cloud) curves in *n*-pentane−polyethylene systems are particularly sensitive to very small differences in the parameters used to describe polyethylene. It is therefore crucial that the correlations are determined as accurately as possible. We are presenting the following refined correlations for the molecular weight dependence of the *n*-alkane parameters to ensure an optimal description of both vapor−liquid and liquid−liquid equilibria:

$$m = 0.02376\ \text{MW/(g mol}^{-1}) + 0.6188 \quad (8)$$

$$m\lambda = 0.04024\ \text{MW/(g mol}^{-1}) + 0.6570$$

$$m(\sigma/\text{Å})^3 = 1.53212\ \text{MW/(g mol}^{-1}) + 30.753$$

$$m(\epsilon/k)/\text{K} = 5.46587\ \text{MW/(g mol}^{-1}) + 194.263$$

where MW is the molecular weight of the alkane in g/mol. The inter-segmental parameters take on asymptotic values when the molecular weight is very large (MW → ∞). This limit provides the following optimal parameters for polyethylene: m = 0.02376 MW/(g mol^{-1}), σ = 4.010 Å, ϵ/k = 230.04 K, and λ = 1.694. Average values of the parameters (σ = 4.025 Å, ϵ/k = 265 K, and λ = 1.614) were used to describe the polymer in a previous study of the absorption of hydrocarbons in polyethylene,[56] instead of the current approach where the values are obtained from the limiting behavior of the correlations. As we have already mentioned these differences are not significant in a description of gas absorption, but will be important if one is interested in the cloud-curve behavior.

2.2 Mixtures of *n*-Alkanes and Polyethylene. A convenient starting point to assess the adequacy of our parameters for polyethylene is to predict the phase behavior of well characterized alkane−polyethylene systems, and in particular the liquid−liquid immiscibility (cloud curves). A number of experimental studies have been undertaken for solutions of short chain hydrocarbons in polyethylene, as polyethylene was one of the first synthetic polymers. A problem with polyethylene, however, is that it is not usually well-defined in terms of branching and polydispersity, and one has to be careful with the reliability of the experimental data. In most theoretical studies of the cloud curves of polymer solutions, adjustable unlike interaction parameters (k_{ij}s) are used, and these are generally taken to be temperature (and in some cases composition and even density) dependent; these are fitted to the experimental data. A good description of the fluid-phase behavior is usually obtained with this kind of approach (e.g., see refs 30, 31, 91, 92). The dependence of the cross parameters on temperature is difficult to predict a priori, and it limits the transferability of the parameters for truly predictive applications.

The adequacy of the SAFT-VR approach in predictions of the fluid-phase equilibria of polyethylene solutions is examined by using the combining rules of Lorentz and Berthelot (no cross interaction parameters, $k_{ij} = 0$). The pure component parameters used for the small *n*-alkanes are those given in Table 1. The parameters for the LDPE and HDPE polymers correspond to the high molecular weight limit obtained from eq 8 (namely, m = 0.02376 MW, σ = 4.010 Å, ϵ/k = 230.04 K, and λ = 1.694); clearly the segment−segment intermolecular parameters are fixed for all of the polyethylenes and only the number of segments vary according to the molecular weight of the polymer.

We first consider *n*-pentane−polyethylene systems for which extensive and reliable experimental data are

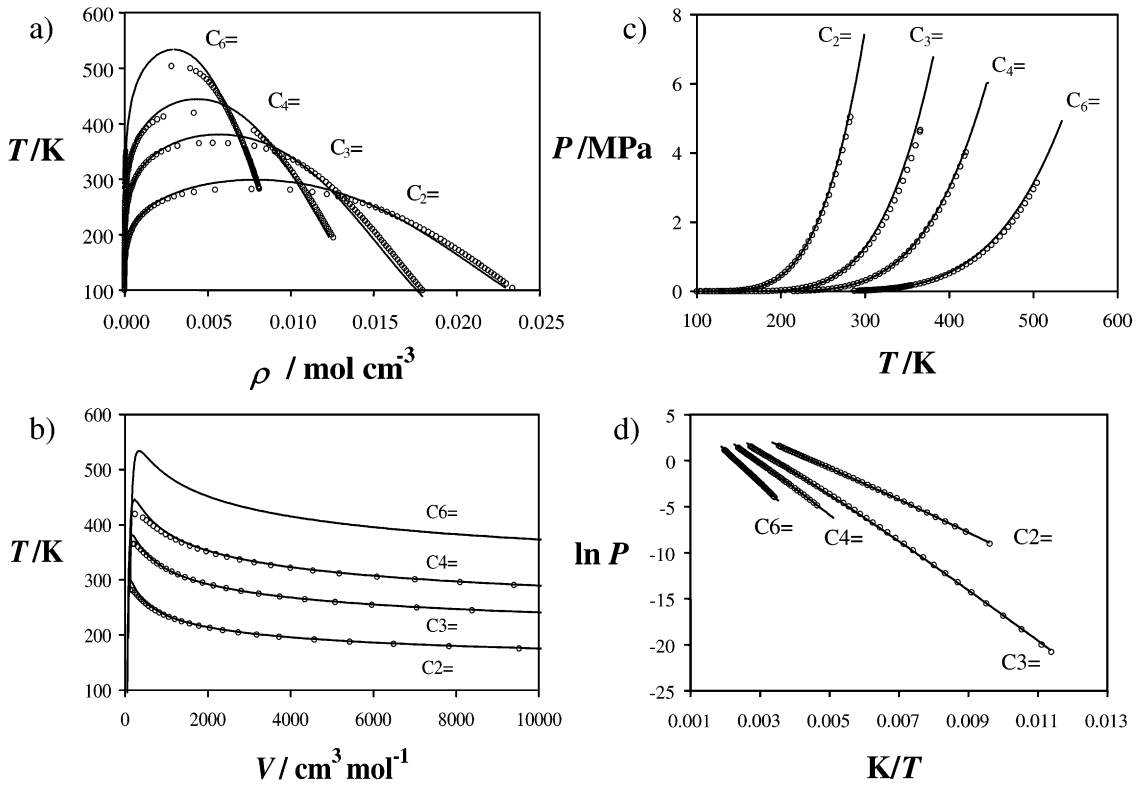

Figure 1. Vapor−liquid equilibria of ethylene (C_2=), propene (C_3=), but-1-ene (C_4=), and hex-1-ene (C_6=): (a) coexistence densities; (b) coexistence volumes; (c) vapor pressures; and (d) Clausius−Clapeyron representation. The circles (○) represent the experimental data[89] and the continuous curves are determined from the SAFT-VR description.

available.[93−96] The calculated pressure−temperature (*PT*) projections of the fluid-phase equilibria for binary mixtures of pentane and long *n*-alkanes, and pentane and polyethylene are depicted in Figure 2a. The *PT* projections for these mixtures are very similar to those obtained for the prototype polymer solutions discussed in reference 9. The fluid-phase behavior is bounded at lower temperatures (∼400 K), below which the system starts to crystallize, and at higher temperatures (∼650 K), above which the alkyl chains decompose. The lower temperature branches of the critical lines (dashed curves in Figure 2a) correspond to loci of lower critical solution temperatures (LCSTs), i.e., to the limits of miscibility of the polymer solution. An additional region of liquid phase demixing bounded by upper critical solution temperatures (UCSTs) is also predicted by the theory at very low temperatures (off the scale of the figure at 40 K); the UCST region is not shown as it is well below the melting points of both pentane and the polymer and most certainly corresponds to metastable fluid phases. In terms of the classification of Scott and van Konynenburg,[97] this type of *PT* projection of the fluid-phase equilibria (with distinct LCST and UCST regions) corresponds to type IV behavior; one could also classify the fluid-phase behavior of this system as type V (LCST behavior only) as the fluid-phase UCSTs are metastable relative to the solid phase. Type IV behavior (or type V depending on one's preference) is always predicted for solutions of polyethylene in pentane, at least within our SAFT-VR approach, even for very high molecular weights of the polyethylene (up to 500 kg mol^{-1}). As the asymmetry between pentane and polyethylene is increased, the region of liquid−liquid immiscibility becomes more extensive and the LCST boundary moves to lower temperature, eventually tending to a limiting value; the LCST region never meets the UCST region predicted at very low temperature (this would correspond to a transition to type III phase behavior[97]). The absence of UCST behavior for polyethylene−pentane in the stable fluid region of the *PT* diagram is in line with experimental observations.

The fluid-phase behavior is qualitatively different for mixtures of polyethylene and methane. Mixtures of asymmetric hydrocarbons have been studied extensively by researchers in Delft,[98−103] who have beautifully mapped out the vapor, liquid, and solid phase behavior of these systems. Though the equilibria between fluid phases becomes metastable at lower temperatures with the formation of solids, de Loos and co-workers[99,101] have pointed out that the fluid-phase behavior for methane−alkanes can be classified as either type III or type IV depending on the asymmetry. We also predict a change from type IV to type III phase behavior (where the LCST and UCST critical lines have merged) for methane−alkane mixtures as the molecular weight of the alkane is increased (see Figure 2b). The fact that the vapor pressure curve of methane is at much lower temperature brings the LCST and UCST regions closer together, enabling them to merge even for relatively short hydrocarbons. In reality a large portion of the critical lines shown in Figure 2b will be masked by the solid phases, so the predictions represent a "model" mixture in which solidification has been suppressed. It is, however, useful to compare this behavior with that found for the mixtures containing pentane (cf Figure 2a) which never exhibit type III behavior. The precise carbon number at which the transition from type IV to type III is predicted for the methane−alkane mixtures is not expected to be quantitatively accurate because the parameters of the components have not been adjusted

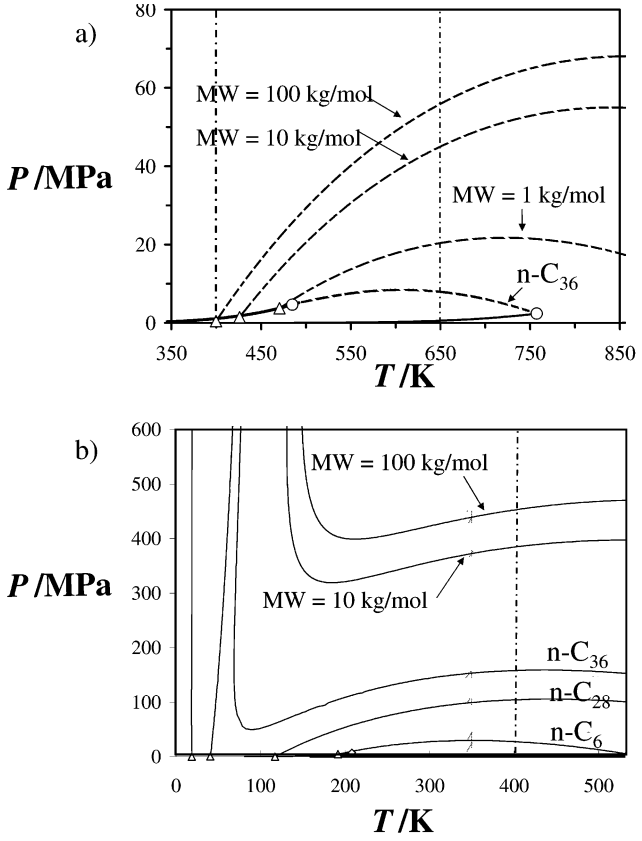

Figure 2. (a) Pressure−temperature *PT* projection of the fluid-phase equilibria for the binary mixtures pentane−*n*-C_{36} and pentane−polyethylene (molecular weight MW = 1, 10, and 100 kg mol^{-1}) predicted with the SAFT-VR approach. The triangles (△) denote the calculated lower critical end points. The continuous curves correspond to the vapor pressure curves of the pure compounds, and the dashed curves correspond to critical lines. The dashed−dotted lines bound the temperature range where the fluid phases are expected to be stable: the lower temperature line roughly denotes the onset of cystallization, and the line at higher temperature is the point at which the alkyl chains start to decompose. An additional UCST region of liquid−liquid immiscibility which appears at 40 K is not shown (cf. part b). (b) Corresponding *PT* projection for the binary mixtures methane−*n*-C_6, methane−*n*-C_{28}, methane−*n*-C_{36}, and methane−polyethylene (MW = 10 and 100 kg mol^{-1}) predicted with the SAFT-VR approach. The curves correspond to the critical lines.

to give a good description of the critical behavior; experimental studies suggest that methane−eicosane (C_{20}) already exhibits type III behavior[99] though this is difficult to confirm due to the metastability of the fluid-phase equilibria. We do, however, expect the general trends to be reproduced by the theory. It is also interesting to note that type III fluid-phase behavior of this kind is also found in mixtures of poly(dimethyl siloxane) and carbon dioxide.[104]

We now return to the fluid-phase equilibria for polymer solutions in pentane. Following previous work,[56] the vapor−liquid equilibria exhibited by mixtures of pentane and polyethylene is obtained by assuming that no polymer molecules are present in the vapor phase and that the polymer is monodisperse. The polydispersity in the molecular weight of the polymer has little effect on the vapor−liquid equilibria, but the effect on the liquid−liquid equilibria can be very significant. The polyethylene polymers that are examined here have an index of polydispersity close to 1, so the effects will be small. Good agreement with the experimental data of

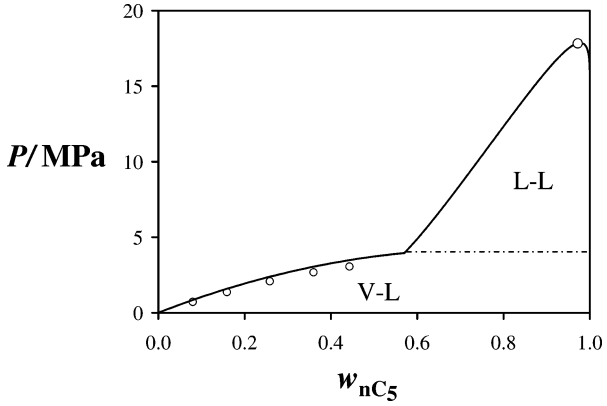

Figure 3. Pressure−composition slice of the vapor−liquid (V−L) and liquid−liquid (L−L) fluid-phase equilibria obtained for the *n*-pentane−polyethylene (LDPE, MW = 76 kg mol^{-1}) system at a temperature of T = 474 K. The weight fraction of pentane is denoted by w_{nC_5}. The vapor−liquid coexistence predicted with the SAFT-VR approach (continuous curves) is compared with experimental data[96] (○). The circle shown at high pressure denotes the calculated upper limit of liquid−liquid immiscibility (UCSP). The dashed line represents the vapor−liquid−liquid three-phase line. No adjustment of the binary interaction parameter is made in these calculations (i.e., $k_{ij} = 0$).

Surana et al.[96] is found for the SAFT-VR predictions of the vapor−liquid equilibria of pentane−PE MW = 76 000 g mol^{-1} (see Figure 3). This corresponds to a fluid state as the temperature of 474 K is above the melting point of polyethylene. The predicted liquid−liquid coexistence region, which disappears above an upper critical solution pressure (UCSP), is shown in the figure for completeness. We have also compared the SAFT-VR predictions of the liquid−liquid equilibria with the data of Xiong and Kiran.[95] for a polyethylene of higher molecular weight; the results are shown in Figure 4. Good agreement is obtained with the experimental cloud curves for the different pressures (Figure 4a) and molecular weights of polyethylene (Figure 4b) examined. Though some deviations are apparent at large pressure and molecular weight, it is important to stress at this point that no adjustable unlike k_{ij} parameters are used in these calculations. The correlations for the polymer parameters (summarized in eq 8) could be refined to improve the description of the cloud curves: the correlations could be determined by simultaneously optimizing the description of the pure *n*-alkane data, *PVT* data of polyethylene, and the cloud curves of solutions of PE in *n*-alkanes (cf. the studies of Lipson and co-workers[105]). We plan to follow this procedure in future studies.

As we mentioned earlier a small change in the segment−segment potential parameters of the polymer can have a large effect on the cloud curve behavior. In particular, a small change in the depth of the potential ϵ_{22} for the polymer segments has a big effect on the calculated cloud curve, as shown in Figure 5a: a 2% decrease in ϵ_{22} shifts the LCST upward by more than 10 K. This effect has also been noted by Lipson et al.[105,106] The different types of segment−segment attractions between solvent−polymer and polymer−polymer molecules are summarized in Figure 5b. The overall attractive energy between a polymer and monomeric solvent is proportional to the chain length through $m_2\epsilon_{12}$, while the energy for a polymer−polymer interaction is proportional to $m_2^2\epsilon_{22}$. As the chain length of the polymer is of the order of $m_2 = 1000$

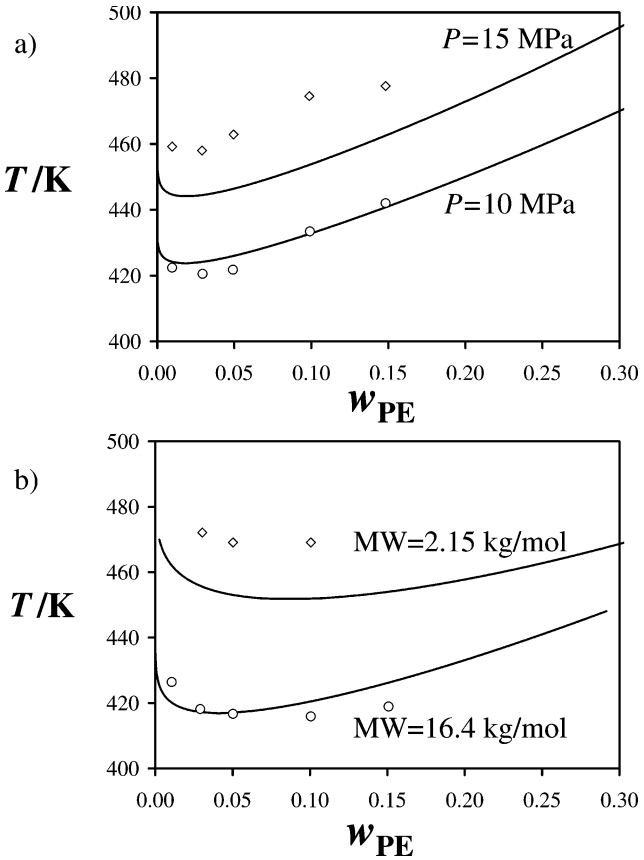

Figure 4. Effect of pressure and molecular weight on the liquid−liquid phase equilibria of polyethylene solutions in pentane: (a) cloud curves for polyethylene with a molecular weight of MW = 108 kg mol^{-1} at pressures of P = 10 and 15 MPa; (b) cloud curves for polyethylene with molecular weights of MW = 2.15 and 16.4 kg mol^{-1} at a pressure of P = 5 MPa. The symbols represent the experimental data of Xiong and Kiran,[95] and the continuous curves are the SAFT-VR predictions. No adjustment of the binary interaction parameter is made in these calculations (i.e., k_{ij} = 0).

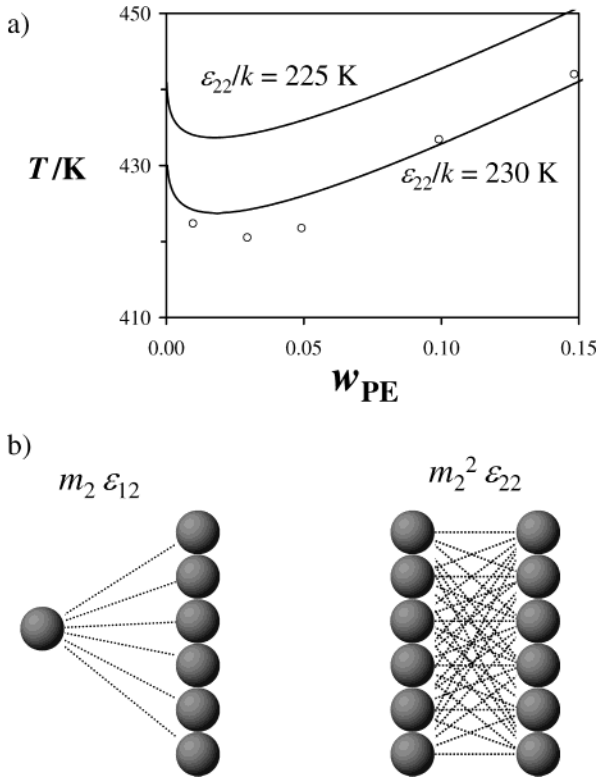

Figure 5. (a) Effect of the segment−segment attractive interaction parameter of the polymer (ϵ_{22}) on the cloud curve calculated with SAFT-VR approach for pentane−polyethylene (MW = 108 kg mol^{-1}) at a pressure of P = 10 MPa compared with the experimental data of Xiong and Kiran[95] (○). (b) Schematic representation of the attractive interactions between solvent−polymer and polymer−polymer segments. The overall attractive energy for the solvent−polymer interactions involves a factor $m_2\epsilon_{12}$, while that for the polymer−polymer interactions involves factor $m_2^2\epsilon_{22}$, m_2 is the number of segments in the polymer chain. A small change of ϵ_{22} gives rise to significant shift in the LCST.

segments, small changes in ϵ_{22} (and to a lesser degree ϵ_{12}) make a big change to the total attractive energy and thus to the phase behavior.

We have also examined the effect of the molecular weight of the *n*-alkane solvent on the LCST of the polyethylene solutions using the same (transferable) parameters for the polymer, and the Lorentz−Berthelot combining rule (k_{ij} = 0). It is well-known that heavier (longer) hydrocarbons are more compatible with polyethylene, and as a consequence the LCST will increase with the chain length of the alkane. We have compared the experimental LCSTs[107−110] with the predictions of our SAFT-VR approach and the BYG theory of Lipson and co-workers.[105] It can be seen from Figure 6 that both approaches provide a good overall description of the LCSTs of the systems; the SAFT-VR predictions are slightly more accurate for the shorter *n*-alkanes, while the BYG theory is more accurate for the larger *n*-alkanes. It is important to point out that some of the deviations from the experimental data may be due to the presence of polydispersity and branching in the experimental samples which are not taken into account in the theoretical approaches. In this context one should also acknowledge the work of de Loos et al.[111] who have used the perturbed hard chain theory (PHCT) to describe LCST behavior for polyetheylene solutions in hydrocarbons.

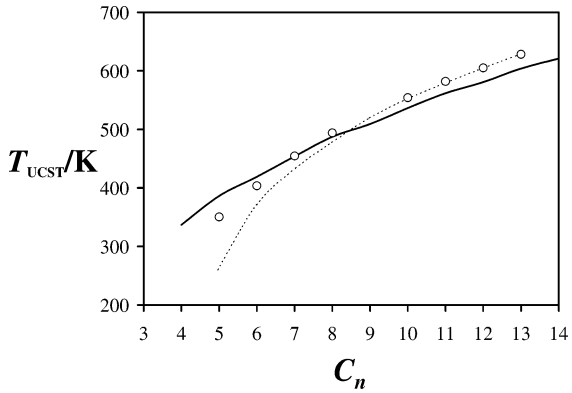

Figure 6. Effect of the chain length C_n of the *n*-alkane solvent on the LCST of mixtures of *n*-alkane−polyethylene (MW = 140 g mol^{-1}). The predictions of the SAFT-VR theory (continuous curve) and the BYG theory[105] (dashed curve) are compared with experimental data[107−110] (○). No adjustment of the binary interaction parameter is made in these calculations (i.e., k_{ij} = 0).

The findings reported in Figures 3−5 confirm the validity of the SAFT-VR approach in describing the fluid (vapor−liquid and liquid−liquid) phase equilibria of alkanes and polyethylene, and the adequacy of the intermolecular parameters developed in this work. In the following sections we use the SAFT-VR approach to examine the solubility of various gases in amorphous and crystalline polyethylene samples in more detail.

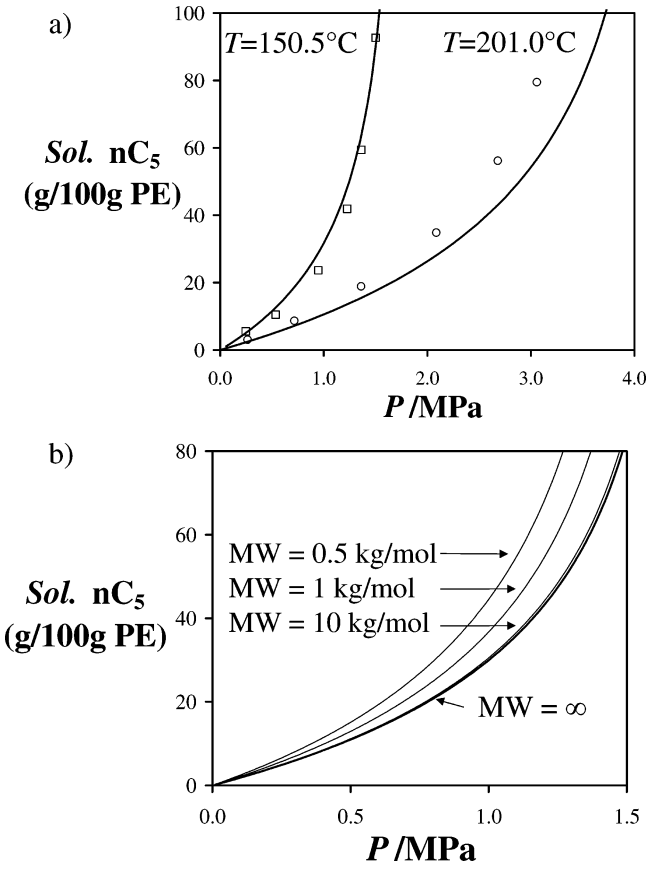

Figure 7. (a) Solubility of *n*-pentane in amorphous polyethylene (LDPE, MW = 76 kg mol^{-1}). The SAFT-VR predictions of the vapor−liquid equilibria (continuous curves) are compared with experimental data[96] at temperatures of T = 150.5 and 201.0 °C. (b) Solubility of *n*-pentane in polyethylene predicted with SAFT-VR at T = 150.5 °C for different molecular weights of the polyethylene. The thick line represents the limiting absorption curve of *n*-pentane in an infinitely long and linear polyethylene. No adjustment of the binary interaction parameter is made in these calculations (i.e., $k_{ij} = 0$).

2.3 Solubility of Gases in Amorphous Polyethylene. The solubility (*Sol.*) of a gas in a polymer is defined as the mass of absorbed gas m_{gas} for a given mass of polyethylene m_{PE} (in percent), and is given by

$$Sol. = 100\frac{m_{gas}}{m_{PE}} = 100\frac{w_{gas}}{w_{PE}} \qquad (9)$$

where w_{gas} and w_{PE} are the weight fractions of gas and polymer in the amorphous (liquid) phase. The absorption curve (solubility as a function of pressure) corresponds to the bubble point curve (pressure as a function of gas weight fraction) of the vapor−liquid equilibria for the gas−polymer mixture. As can be seen from Figure 7a (and the corresponding Figure 3) the absorption curves of the system *n*-pentane−polyethylene are well predicted by the SAFT-VR approach at several temperatures without the need for adjustable binary parameters ($k_{ij} = 0$). The solubility of the gas is found to decrease as the molecular weight of polyethylene is increased as shown in Figure 7b. This is due to an increase in the incompatibility between the gas and the polymer as the difference in size becomes larger (see ref 9 for further explanations). The effect of changing the molecular weight of polyethylene on the vapor−liquid coexistence curve is, however, relatively small compared to its effect on the liquid−liquid coexistence curve (see Figure 4b). The absorption curves rapidly tend to a limiting curve as the molecular weight of polyethylene is increased. When the chain length is large enough, the solubility of the gas is no longer affected, as the gas molecules interact with the polymer at the level of the polymer segments when they absorb in the liquid phase. The absorption curve is, for practical purposes, indistinguishable from that of the infinite polymer limit for molecular weights higher than about 5 kg mol^{-1}. In our studies we have not found the need to incorporate the effect of the chain architecture explicitly (see the recent simulation study by Banaszak et al.[112]).

We have also examined the solubility of two small gas molecules (ethylene and nitrogen) in amorphous polyethylene using SAFT-VR. In the case of these systems, an adjustment of the cross interaction parameter k_{12} is required for an accurate representation of the fluid-phase equilibria. The combining rules for these small molecules deviate from the Lorenz−Berthelot rule because of the difference in the intermolecular interactions energies with the alkanes. However, a single cross interaction parameter for each gas is sufficient to predict the solubility over a large range of temperatures. We have used $k_{12} = 0.075$ for ethylene−polyethylene, and $k_{12} = 0.15$ for nitrogen−polyethylene. The value of the cross interaction parameter in the mixtures involving nitrogen is quite large, but consistent with that of a more polar compound; values of this magnitude have been previously reported for studies of vapor−liquid equilibria of mixtures of alkanes and nitrogen with PC-SAFT.[113] The experimental absorption curves[114,115] are well represented by the SAFT-VR equation of state for both gases. It is clear from Figures 7a and 8 that the solubility of the gas at a given pressure is greater when the gas is less volatile (has a higher molecular weight). The solubilities are thus ranked in the following decreasing order: $Sol._{nC_5} > Sol._{C_2=} > Sol._{N_2}$.

The solubility of a gas in polyethylene usually decreases with increasing temperature (see pentane−polyethylene in Figure 7a and ethylene−polyethylene in 8a). This is because the gas becomes less volatile when the temperature is decreased: in keeping with other high temperature perturbation expansions, the attractive term of the gas in the SAFT-VR free energy is inversely proportional to temperature ($\sim\epsilon_{11}/kT$) so the lower the temperature, the stronger the attractions, and the less volatile the gas. In this case the attractive contribution to the free energy dominates the ideal free energy of the mixture; the ideal entropy of mixing term favors a higher solubility (mixing) at higher temperature. Moreover, the absorption curve is concave, and its concavity increases as the gas becomes less volatile. This feature is analogous to the phenomenon of condensation which occurs when a gas adsorbs on the surface of solids. In the case of the *n*-pentane−PE mixtures, the liquid phase comprises both species (pentane and polymer molecules). As the pentane molecules progressively absorb in the liquid phase, they encounter more and more pentane molecules; the pentane−pentane interactions are attractive and more favorable than the pentane−polymer segment interactions so that there is a synergy, and the absorption curve increases progressively (and reaches a limit close to the saturation point). The ethylene−ethylene attractive interactions are not as strong as the pentane−pentane interactions, and the synergy is less pronounced: the pressure dependence

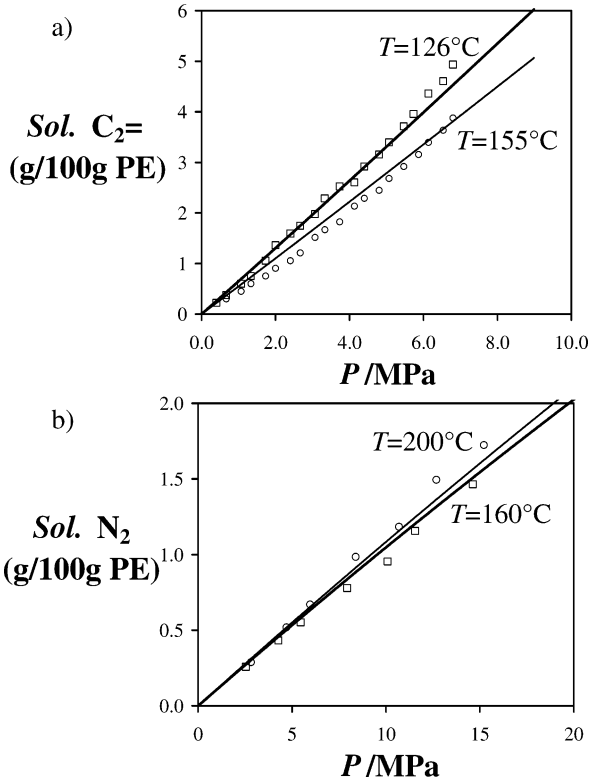

Figure 8. (a) Solubility of ethylene (C_2=) in amorphous polyethylene (LDPE, MW = 248 kg mol^{-1}). The SAFT-VR predictions of the vapor−liquid equilibria (continuous curves) are compared with experimental data[114] at temperatures of T = 126 and 155 °C. One binary interaction parameter k_{12} = 0.075 is used for all temperatures (cf. ref 56). (b) Solubility of nitrogen (N_2) in amorphous HDPE (MW = 111 kg mol^{-1}). The SAFT-VR predictions (continuous curves) are compared with experimental data[115] at temperatures of T = 160 and 200 °C. In this case a binary interaction parameter of k_{12} = 0.15 is used.

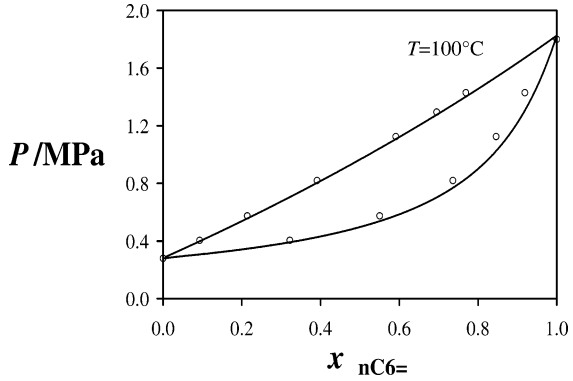

Figure 9. Pressure−composition Px slice of the vapor−liquid-phase equilibria for the but-1-ene−hex-1-ene binary mixture at a temperature of T = 100 °C. The circles (○) denote experimental data[116] and the continuous curves represent the SAFT-VR predictions.

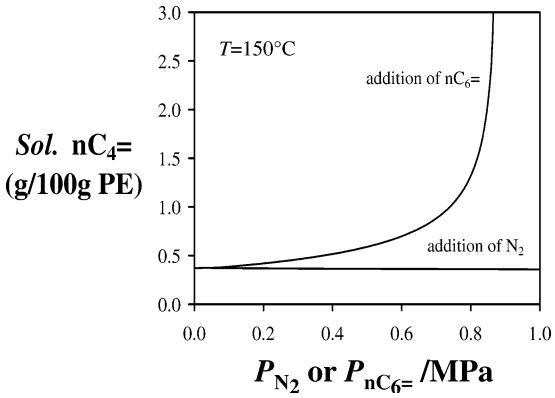

Figure 10. SAFT-VR predictions for the solubility of but-1-ene in amorphous polyethylene (HDPE, MW = 100 kg mol^{-1}) at a temperature of T = 150 °C and fixed partial pressure of but-1-ene $P_{nC_4=}$ = 0.05 MPa, as a function of the partial pressure of a second gas (nitrogen or hex-1-ene).

of the solubility curve of ethylene is almost linear (see Figure 8a) and Henry's law could be applied.

It is interesting to note that in the case of nitrogen, the absorption curve is convex (see Figure 8b). Furthermore, the solubility of nitrogen in polyethylene increases with increasing temperature, contrary to what is found in the case of pentane and ethylene. This experimental observation is predicted by the SAFT-VR approach (see Figure 8b). The finding can be explained as follows: at "high" temperatures, the nitrogen−nitrogen interactions are almost purely repulsive (at these conditions nitrogen is significantly supercritical and behaves almost like a hard dumbbell). In this case, the presence of nitrogen in the liquid phase increases the repulsive interactions and as a consequence does not favor the solubility of the gas, leading to a convex curve. The attractive terms in the free energy are very small and dominated by other terms such as the ideal free energy term. Due to the ideal entropy of mixing, the nitrogen molecules tend to mix more with polyethylene molecules at higher temperatures and the solubility increases. These "high" temperatures correspond to the far supercritical region of the pressure temperature PT diagram of N_2−PE: in this region the vapor−liquid critical pressures of the mixture decrease as the temperature is increased, which is consistent with the evolution of the nitrogen solubility.

2.4 Co-Absorption of Gases in Amorphous Polyethylene. The effects of the co-absorption of a number of gases in a polymer represent an important industrial problem: the solubilities of the different gases determine the rate of a gas phase polymerization reaction, and hence the final composition (structure) of the monomers forming the polymer chain. We consider here the ternary systems but-1-ene−nitrogen−HDPE and but-1-ene−hex-1-ene−HDPE. The binary system but-1-ene−hex-1-ene behaves almost like an ideal mixture, and so there is no need to use an adjustable parameter to accurately describe the experimental vapor−liquid equilibria[116] (see Figure 9). Similarly, no cross interaction parameters are used for the binary system but-1-ene−N_2, though at higher partial pressures of nitrogen this may be necessary. In the case of the interactions between the smaller molecules and PE the following binary parameters are employed: k_{ij} = 0 for the but-1-ene−PE and hex-1-ene−PE systems; k_{ij} = 0.15 for the N_2−PE system.

We first consider the change in the solubility of but-1-ene in PE when a second gas (hex-1-ene or nitrogen) is added. The partial pressure (gas-phase composition) of but-1-ene is fixed, and the partial pressure of the second gas is increased. In this discussion, we neglect the effects of the interactions between the molecules in the vapor phase, and one can examine the behavior simply in terms of the partial pressure of each gas. The SAFT-VR predictions are presented in Figure 10. A very different behavior is observed depending on whether hex-1-ene or nitrogen is added as the co-absorbant: the presence of nitrogen hardly affects the solubility of but-

1-ene in PE (the solubility slightly decreases), while an increase in the partial pressure of hex-1-ene leads to a dramatic increase in the solubility of but-1-ene. Such effects have been observed experimentally[79] and predicted by Monte Carlo simulation,[13,80] but have not been explained in terms of the intermolecular interactions.

In the case of the ternary system but-1-ene−nitrogen−polyethylene at temperatures of about 400 K, nitrogen behaves almost as a hard dumbbell, and the nitrogen−nitrogen and but-1-ene−nitrogen interactions are almost purely repulsive. There is a slight absorption of nitrogen in the liquid polyethylene phase due to the ideal entropy of mixing. When the but-1-ene molecules absorb in the liquid phase, they encounter a mixture of but-1-ene, nitrogen, and polyethylene. Because the interactions between but-1-ene and nitrogen are much less favorable than those between but-1-ene molecules, and between but-1-ene and polyethylene, the presence of nitrogen decreases the solubility of but-1-ene for a fixed partial pressure of but-1-ene. The decrease of solubility is very small because nitrogen only absorbs weakly in polyethylene.

As far as the system but-1-ene−hex-1-ene−polyethylene is concerned, the interactions between but-1-ene and hex-1-ene are attractive and very similar to the interactions between but-1-ene. When the partial pressure of hex-1-ene is increased, the solubility of hex-1-ene in the liquid polyethylene phase increases dramatically. The presence of hex-1-ene in polyethylene gives rise to an increase in the solubility of but-1-ene and to a concave absorption curve because the interactions between but-1-ene and hex-1-ene are more favorable than the interactions between but-1-ene and the polymer (see Figure 10). Ternary diagrams of the system but-1-ene−hex-1-ene−amorphous HDPE have been determined with the SAFT-VR approach at $T = 460$ K, and pressures $P = 1$ MPa (Figure 11a) and $P = 3$ MPa (Figure 11b). At the lower pressure, a broad vapor−liquid region can be seen and the solubility of both olefins in the polymer is low. When the pressure is increased, the fluid-phase diagram changes dramatically as regions of liquid−liquid immiscibility appear (corresponding to coexistence between a phase rich in polymer and a phase rich in hex-1-ene). The binary mixtures hex-1-ene−PE and but-1-ene−PE are both found to exhibit type IV fluid-phase behavior (with separate regions of UCST and LCST liquid−liquid immiscibility). The temperature chosen for the ternary diagrams depicted in Figure 11 is above the LCEP of the binary mixtures. Although hex-1-ene is more miscible in the polymer than but-1-ene, the liquid−liquid immiscibility in the ternary mixture first occurs in the region rich in hex-1-ene (see Figure 11b). This is because at a given temperature the vapor pressure of hex-1-ene is lower than that of but-1-ene, and as the liquid−liquid-vapor three-phase line of each binary mixture is very close to the vapor pressure curve of the solvent, a hex-1-ene rich liquid will be the first to form.

The solubility of hex-1-ene gas in polyethylene increases markedly as one goes from vapor−liquid to liquid−liquid equilibrium. It is also clear that the concentration of but-1-ene in both of the coexisting liquid phases is relatively high. A knowledge of this type of fluid-phase behavior could be used to design separation processes in polymer systems by taking advantage of the large changes in the weight fractions of a given gas in the polymer with pressure.

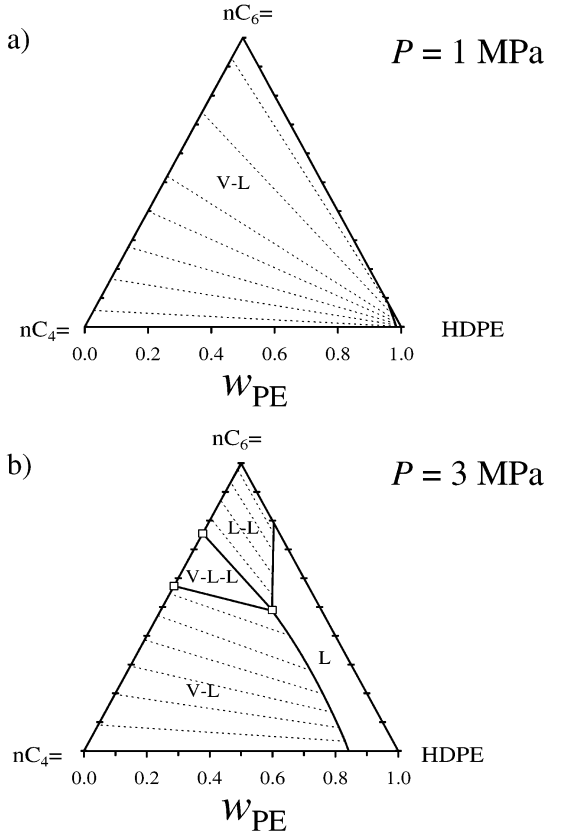

Figure 11. SAFT-VR predictions for the ternary fluid-phase diagrams of the system but-1-ene−hex-1-ene−amorphous polyethylene (HDPE, MW = 100 kg mol^{-1}) at a temperature of $T = 460$ K and pressures (a) $P = 1$ MPa, and (b) $P = 3$ MPa. The compositions are represented in terms of the weight fractions w_i of each component. Vapor−liquid (V−L), liquid−liquid (L−L), and vapor−liquid−liquid (V−L−L) three-phase equilibria can be seen. The continuous lines represent the coexistence curves and the dashed lines are the tie lines. The squares denote the calculated three phase points.

3. Crystallinity of Polyethylene

In the previous sections the polyethylene samples are assumed to be an amorphous fluid; the high-temperature states examined ensure that the polymer is molten. At temperatures below ∼130−140 °C polyethylene is semicrystalline. As with other polymers, polyethylene does not exhibit the crystallization behavior of a simple pure component. The presence in the polymer chain of units that differ chemically, stereochemically, or structurally from the predominant chain repeat units restricts the process of crystallization. In the case of a pure component, the Gibbs phase rule of course requires that there is a single melting point T_m for each value of the applied pressure P; if the temperature is just below T_m, the equilibrium state of the pure component sample is a uniform solid, and at a temperature just above T_m the component is fully liquid. A polymer is not however a pure component, but a mixture of compounds varying in size and chemical structure. Moreover, some of the side-groups of the polymer chain, such as the alkyl branches, adversely affect the kinetics of crystallization as they cannot be easily accommodated into a uniform solid structure (at least in the typical time scale of the experiment). The cooling rate and the thermal history of the sample also affect the crystallinity the polymer. One can nevertheless define a pseudo melting point T_m for the polymer sample, which is analogous to the

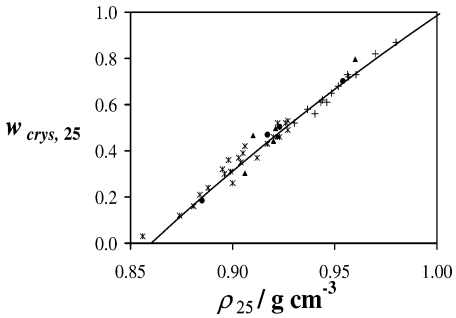

Figure 12. Crystallinity $w_{crys,25}$ at ambient conditions ($T = 25$ °C, $P = 1$ atm) of various polyethylene samples (HDPE, LDPE, and LLDPE) as a function of the polymer density $\rho_{c,25}$ at ambient conditions. The experimental data are from the studies by McKenna[12] (▲), Jordens et al.[61] (+), Moore et al.[2] (●), and Starck et al.[63] (*). The continuous curve corresponds to eq 10 with $\rho_{c,25} = 1.005$ g cm^{-3} and $\rho_{a,25} = 0.862$ g cm^{-3}.

melting point of a pure component, as the point beyond which the polymer sample becomes totally amorphous. At temperatures below this limiting point ($T < T_m$), only a fraction w_{cyrs} of the polymer exists as crystallized units; this fraction is referred to as the crystallinity of the polymer. In this case the polymer sample is semicrystalline, as it consists of amorphous regions which exhibit a liquidlike structure, and ordered crystallized structures called crystallites.

Polyethylene samples are commonly characterized in terms of their density ρ_{25} at ambient conditions. The weight fraction crystallinity $w_{crys,25}$ at ambient condition can be evaluated from the relation[117]

$$w_{crys,25} = \frac{\rho_{25} - \rho_{a,25}}{\rho_{c,25} - \rho_{a,25}} \frac{\rho_{c,25}}{\rho_{25}} \qquad (10)$$

where $\rho_{c,25}$ and $\rho_{a,25}$ are the average densities in (g cm^{-3}) of the crystallites and the amorphous regions also at ambient conditions. Relation 10 is exact as it is derived from a mass balance equation. As a reasonable approximation one can use the same densities $\rho_{c,25}$ and $\rho_{a,25}$ for the different types of polyethylene (HDPE, LDPE, LLDPE) since the properties of these polymers tend to be closely correlated to the relative amounts of the amorphous and crystallite regions. This means that the degree of crystallization in polyethylene can be predicted simply from a knowledge of the overall average density of the polymer sample. One should note that the term "high density" polyethylene (HDPE) refers to highly crystallized polyethylene, but does not mean that the corresponding molten polyethylene has a high density. We propose slightly different values from those of Yiagopoulos et al.[117] for the densities $\rho_{c,25}$ and $\rho_{a,25}$ after re-correlating the experimental data[2,12,61,63] of different types of polyethylene: $\rho_{c,25} = 1.005$ g cm^{-3} and $\rho_{a,25} = 0.862$ g cm^{-3}. It can be seen from Figure 12 that the agreement between the experimental data and relation 10 is good. Significant deviations (max 12%) are observed for a few of the polymer samples, which may be due to the assumption that $\rho_{c,25}$ and $\rho_{a,25}$ are the same for all of the samples, or due to inaccuracies in the measurements.

3.1 Flory Theory of Polymer Crystallization. The most rigorous theory for the prediction of the temperature dependence of the crystallinity of polymer samples at equilibrium was developed about fifty years ago by Flory.[69] An assessment of the adequacy of the theory is, however, very scarce (see refs 71 and 72), partially due to the fact that accurate techniques to measure the crystallinity of a polymer sample as a function of temperature have only been developed in recent years.[12,63] The Flory approach is based on the following arguments: the crystallinity w_{crys} represents the weight fraction of crystallized polymer in the sample; as the mass of a polymer molecule is proportional to the number of units in the chain (the proportionality factor is the molecular weight of the monomer), the crystallinity also corresponds to the probability that a given polymer unit crystallizes on cooling. In the Flory theory, one defines a "copolymer" as any polymer containing different types of units along the main chain. For instance, polyethylene which is synthesized from ethylene can be treated as a "copolymer" since it contains both crystallizable ethylene groups and non-crystallizable units such as those on the alkyl branches along the chain. The ethylene groups between two close branches are inaccessible because of the entanglement of the chains.

Following Flory's development, we consider a model polymer which contains crystallizable units designated by "A", and non-crystallizable units designated by "B". The crystallinity w_{crys} is defined as the mass of crystallized polymer in the sample, which is also the fraction of crystallized polymer units at equilibrium. One should not confuse w_{crys} with the fraction of crystallizable units A in the chain, $X_A = 1 - X_B$. The frequency (connectivity) of A units along the chain is also an important factor. A block copolymer has a higher crystallinity than an alternating copolymer, as the probability that a block of consecutive A units crystallizes increases with an increase in the number of consecutive A units in the block. One can define a probability p that a given A unit in the chain is followed by another A unit along the same chain (in any direction). The probability p is used as an average, independently of the direction and the position of the A unit in the chain. This probability p provides a quantitative differentiation between random-, alternating-, and block-type copolymers: for random copolymers, p corresponds to the fraction of A units $p = X_A$; for block copolymers, p greatly exceeds X_A ($p \sim 1$), as the A units are more likely to be in blocks; for alternating copolymers, p is around zero as each A unit is adjacent to two B units. Flory's theory is a one-dimensional theory where crystallization occurs along a unique infinitely long chain. For practical purposes, however, one can assume that p represents the probability of finding two consecutive crystallizable A units within adjacent chains in three dimensions. As a result, the probability p indirectly characterizes the cooling rate. For low cooling rates, the chain molecules have more time to arrange themselves to form large blocks of crystallizable A units (corresponding to higher values of p) and reach configurations of lower free energy. In the case of a high cooling rate, the formation of blocks of A units within several chains is limited by the kinetics and the entanglement of the chains, leading to lower values of p.

In Flory's theory the longitudinal development of the crystallites is restricted by the occurrence of non-crystallizable B units along the polymer chain. The lateral development is governed by the availability (or concentration) of sequences of suitable length in the residual melt, and by the decrease in free energy that occurs when a sequence of ζ A units is transferred from the amorphous to the crystalline phase.

A useful quantity in the Flory analysis is the probability P_ζ that a given A unit in the amorphous phase is located within a consecutive sequence of at least ζ such A units. A quantitative description can then be developed by relating P_ζ to the melt composition through the overall probability w_ζ that a unit chosen at random from the amorphous regions is an A unit and also that this A unit belongs to a block of exactly ζ A units bounded at either end by B units. It can be shown[57,69] that the probabilities P_ζ and w_ζ are related by

$$w_\zeta = \zeta(P_\zeta - 2P_{\zeta+1} + P_{\zeta+2}) \tag{11}$$

This relationship is universal and independent of the process of crystallization. The quantities P_ζ and w_ζ are related to the composition of both the initial polymer melt and the semicrystalline sample. In the completely molten copolymer, prior to any crystallization, the initial probability w_ζ^0 is given by

$$w_\zeta^0 = \frac{N_{A,\zeta}}{N} \tag{12}$$

where $N_{A,\zeta}$ is the number of A units in the molten polymer belonging to blocks (or sequences) containing exactly ζ consecutive A units, and $N = A + B$ is the total number of units. If ν_ζ^0 is the number of sequences of ζ A units in the molten polymer, such that $N_{A,\zeta} = \zeta\nu_\zeta^0$, and $N_A = X_A N$ (where N_A and X_A are the total number and mole fraction of A units respectively), then w_ζ^0 can be written as

$$w_\zeta^0 = \frac{X_A \zeta \nu_\zeta^0}{N_A} \tag{13}$$

By assuming that the probability p of an A unit being succeeded by another A unit is independent of the number of preceding A units in the sequence, one can write eq 13 in the usual Flory−Huggins form as

$$w_\zeta^0 = \frac{X_A \zeta (1-p)^2 p^\zeta}{p} \tag{14}$$

By combining eqs 11 and 14, the probability P_ζ^0 that in the initial amorphous state a given A unit belongs to a sequence of at least ζ units can be written as

$$P_\zeta^0 = X_A p^{\zeta-1} \tag{15}$$

Relation 15 essentially states that the probability P_ζ^0 is the product of the probability X_A of choosing an A unit from the N total units and the probability that this given A unit is followed by at least $\zeta - 1$ successive A units (each with a fixed probability p).

When crystallization occurs and thermodynamic equilibrium is maintained, the probability P_ζ^{eq} that a given A unit in the amorphous regions is located in a sequence of at least ζ units is directly proportional to the Boltzmann factor of the change of free energy due to the fusion of a block of ζ units:

$$P_\zeta^{eq} = e^{-\Delta G_\zeta / RT} \tag{16}$$

where ΔG_ζ is the free energy of fusion per mole of a sequence of ζ units A (from a mole of crystallized ζ units A). This type of relation is common in statistical thermodynamics (see, for example, the free energy change on particle insertion as described by the potential distribution theorem of Widom[118]). The change in free energy ΔG_ζ can be expressed as

$$\Delta G_\zeta = \zeta \Delta G_u - 2\sigma_e \tag{17}$$

where $\Delta G_u = \Delta H_u - T\Delta S_u$ is the free energy of fusion per mole of units, and σ_e is the surface free energy associated with a mole of terminal units at the end of the crystallites. For polyethylene, one can take the values $\sigma_e/R = 1190.7$ K, where R is the gas constant ($R = 8.314411$ J mol^{-1} K^{-1}); $\Delta H_u/R = 996.34$ K, and $\Delta S_u = \Delta H_u/T_m^0$, where T_m^0 is the melting point of an ideal totally crystallizable polyethylene (see references 63, 71, and 72). In this treatment, one assumes that ΔH_u is constant in the range T to T_m^0. Equation 16 can be expressed as

$$P_\zeta^{eq} = D^{-1} e^{-\zeta\theta} \tag{18}$$

where

$$\theta = \frac{\Delta H_u}{R}\left(\frac{1}{T} - \frac{1}{T_m^0}\right), \tag{19}$$

and

$$D = e^{-2\sigma_e/RT} \tag{20}$$

Equations 11 and 18 can then be combined to give

$$w_\zeta^{eq} = \zeta D^{-1}(1 - e^{-\theta})^2 e^{-\zeta\theta} \tag{21}$$

which represents the fraction of molten A units from sequences of ζ consecutive units. The necessary and sufficient condition that blocks containing ζ A units crystallize is

$$w_\zeta^0 > w_\zeta^{eq} \tag{22}$$

There is a critical length ζ_{crit} under which the blocks do not crystallize. This critical length corresponds to

$$w_{\zeta_{crit}}^0 = w_{\zeta_{crit}}^{eq} \tag{23}$$

and by combining eqs 14 and 21 ζ_{crit} can be expressed as

$$\zeta_{crit} = -\frac{\ln(DX_A/p) + 2\ln((1-p)/(1-e^{-\theta}))}{\theta + \ln p} \tag{24}$$

The inequality $P_{\zeta_{crit}}^0 > P_{\zeta_{crit}}^{eq}$ (cf. eq 22) can be used to determine the melting point T_m of the polymer as follows:

$$\frac{X_A}{p} p^\zeta > \frac{1}{D} e^{-\theta\zeta} \tag{25}$$

Except for copolymers exhibiting a degree of alternation, $1/D$ is greater than X_A/p. The inequality 25 can thus be written as

$$\theta > -\ln p \tag{26}$$

or

$$\frac{1}{T} - \frac{1}{T_m^0} > -\frac{R}{\Delta H_u}\ln p \tag{27}$$

This expression can be used to provide an estimate of the limiting temperature where crystallization occurs. The melting point T_m must satisfy the relation

$$\frac{1}{T_m} - \frac{1}{T_m^0} = -\frac{R}{\Delta H_u}\ln p \tag{28}$$

A further approximation is then made to simplify the analysis: since the values of X_A and p are very similar in practice, one can neglect the term X_A/p in eq 24; the term $\ln (DX_A/p)$ does not have much of an effect on the final crystallinity as shown in ref 57. Equation 24 for the critical number of crystallizable units becomes

$$\zeta_{crit} = -\frac{\ln D + 2\ln((1-p)/(1-e^{-\theta}))}{\theta + \ln p} \tag{29}$$

The temperature $T_m^0 = \Delta H_u/\Delta S_u$ is the melting temperature of the ideal homopolymer. This temperature can be considered as a reference melting point, and takes into account several effects such as the molecular weight, the lamellar thickness, the presence of defects, and chain ends[57]; these are different from other copolymer effects such as branching. To remove the explicit dependence on T_m^0 and hence the dependence on the various effects, one can combine eqs 28, 29, and 19 to give

$$\theta = \frac{\Delta H_u}{R}\left(\frac{1}{T} - \frac{1}{T_m}\right) - \ln p, \tag{30}$$

and

$$\zeta_{crit} = -\frac{\ln D + 2\ln((1-p)/(1-e^{-\theta}))}{\frac{\Delta H_u}{R}\left(\frac{1}{T} - \frac{1}{T_m}\right)} \tag{31}$$

Equation 31 implies that only very long sequences of A units can crystallize when the temperature T is close to the melting point. If w_ζ^{crys} denotes the fraction of sequences of ζ A units which have crystallized, then

$$w_\zeta^{crys} = w_\zeta^0 - w_\zeta^{eq} \tag{32}$$

Applying the properties of mathematical series, the total fraction of crystallized units w_{crys} (crystallinity) can be obtained as

$$w_{crys}(T) = \sum_{\zeta=\zeta_{crit}}^{\infty} w_\zeta^{crys} \tag{33}$$

$$= \frac{X_A}{p}(1-p)^2 p^{\zeta_{crit}}\left[\frac{p}{(1-p)^2} - \frac{e^{-\theta}}{(1-e^{-\theta})^2} + \zeta_{crit}\left(\frac{1}{1-p} - \frac{1}{1-e^{-\theta}}\right)\right]$$

This relation allows one to determine the temperature dependence of the degree of crystallinity from a knowledge of the fractions X_A and p and the thermodynamics of fusion of the chain.

3.2 Predicting the Crystallinity of Polyethylene with a Scaled Flory Approach. The main difficulty in describing the crystallinity of polyethylene is that the exact mole fraction of crystallizable units X_A and probability of finding the appropriate neighboring units p cannot be measured. Moreover, additional dependencies on the molecular weight, lamellar thickness, defects, and chain ends must be included via the reference temperature T_m^0.[70−72] Sanchez and Eby[70] have derived an expression for the melting point taking into account the defects, chain ends, and lamellar thickness. The Sanchez−Eby approach provides a better description of the melting point than the original theory of Flory (see ref 71), but a number of parameters have to be fitted to experimental data, so that the predictive capability of the approach is restricted. The theory of Sanchez and Eby also requires a knowledge of the experimental value of the fraction X_A (or X_B) of ethylene units, which is not always available. Furthermore, the assumption that the polyethylene sample is a random copolymer (i.e., that $p \approx X_A$) may be too crude in the case of block-type copolymers: Ziegler−Natta (ZN) catalysts are found to favor the formation of block-type copolymers, while other catalysts such as metallocenes (Me) favor random-like copolymers.[60,62,63] This means that $p \geq X_A$ for certain kinds of catalysts.

Here, we use the Flory theory to develop a predictive approach for the melting point and crystallinity of an arbirtary polyethylene sample which requires a minimum of experimental data. The density ρ_{25} of a polyethylene sample (measured at 25 °C and 1 atm) is often used to characterize the degree of branching of the polymer:[111] the density ρ_{25} is about 1 g cm^{-3} for a totally crystallized linear polyethylene, and 0.86 g cm^{-3} for a completely amorphous sample. In the case of HDPE, ρ_{25} is 0.96 g cm^{-3}; and in LDPE and LLDPE ρ_{25} is about 0.92 g cm^{-3}. The density ρ_{25} can also be related directly to the crystallinity $w_{crys,25}$ at 25 °C via eq 10, and as a consequence $w_{crys,25}$ can be used as a measure of the branching in the sample. To aid a quantitative description with the Flory approach we ensure that the theory reproduces the experimental values for $w_{crys,25}$. By requiring that eq 33 satisfies the relation $w_{crys}(T = 25) = w_{crys,25}$, the explicit dependence on the mole fraction of crystallizable ethylene units X_A can be removed:

$$w_{crys}(T) = w_{crys,25} p^{\zeta_{crit}}\left[\frac{p}{(1-p)^2} - \frac{e^{-\theta}}{(1-e^{-\theta})^2} + \zeta_{crit}\left(\frac{1}{1-p} - \frac{1}{1-e^{-\theta}}\right)\right]$$

$$\div \left(p^{\zeta_{crit,25}}\left[\frac{p}{(1-p)^2} - \frac{e^{-\theta_{25}}}{(1-e^{-\theta_{25}})^2} + \zeta_{crit25}\left(\frac{1}{1-p} - \frac{1}{1-e^{-\theta_{25}}}\right)\right]\right) \tag{34}$$

where θ_{25} and $\zeta_{crit,25}$ are obtained from eqs 30 and 31 at the temperature $T = 25$ °C. The experimental value of the crystallinity at 25 °C $w_{crys,25}$ can be evaluated from eq 10 if unknown.

Correlations of the melting point and of the probability p are now made solely as a function of $w_{crys,25}$. We have examined such correlations using the experimental data in references 12 and 63 for the two main types of catalyst (ZN and Me) used in polymerization

reactors. The melting points T_m of polyethylene can be described in terms of the following functions of $w_{crys,25}$:

$$T_m/°C = 13.689w_{crys,25}^2 + 5.015w_{crys,25} + 124.33, \text{ for ZN catalysts} \quad (35)$$

$$T_m/°C = -81.498w_{crys,25}^2 + 163.3w_{crys,25} + 63.415, \text{ for Me catalyst} \quad (36)$$

The correlations for the two types of catalysts go through the point for an ideal infinitely long and linear polyethylene molecule ($w_{crys,25} = 1.0$, $T_m = 145$ °C). A parametrization of the probability p in terms of $w_{crys,25}$ can also be obtained using eq 34 and experimental data of w_{crys} with temperature,[12,63] giving

$$p = -0.0581w_{crys,25}^2 + 0.1279w_{crys,25} + 0.9303, \text{ for ZN catalysts} \quad (37)$$

$$p = -0.0538w_{crys,25}^2 + 0.1397w_{crys,25} + 0.9142, \text{ for Me catalysts} \quad (38)$$

As required, the probability p of adjacent crystallizable units is equal to 1 for an ideal infinitely long and linear polyethylene which crystallizes completely, in the case of both the ZN and Me catalysts. The melting point T_m and probability p are depicted in Figure 13a and b, respectively. It can be seen that both the melting point T_m and the probability p are higher for ZN polyethylenes than for Me polyethylenes. This result is in agreement with experimental observations:[60,62,63] the ZN polyethylenes are of the block-copolymer type (higher p) and crystallize more readily (higher T_m) than Me polyethylenes, which are more random-type in nature (lower p).

As a final assessment we examine the predictive capabilities of our scaled Flory theory (eq 34) for the crystallinity of polyethylene using the correlations obtained for T_m and p in terms of $w_{crys,25}$. As can be seen from Figure 14, our general approach accurately describes the crystallinity of a large variety of ZN and Me polyethylenes, including HDPE, LDPE, and LLDPE produced with butene, hexene, or octene as comonomers. Excellent quantitative agreement is obtained: at low temperatures the crystallinity tends to a finite crystallinity, while it decreases exponentially and tends to zero as the temperature is increased toward the melting point T_m. The correlations that have been employed for T_m and p only require the crystallinity of the sample at 25 °C $w_{crys,25}$ as input (a property which is usually accessible), and thus make the approach totally predictive. Note that we have avoided the issues associated with the thermal history of the sample and the cooling rate by expressing the probility p (and melting point T_m) as a function of $w_{crys,25}$: the experimental value of the crystallinity $w_{crys,25}$ which is used as an input parameter already contains the necessary information about the cooling rate. For example, lower cooling rates would give rise to higher $w_{crys,25}$ for the same sample. In view of the fact that polymer samples are often poorly characterized, the purpose here is to develop an approach which is based on a fundamental theory, and at the same time requires the minimum amount of information about the polymer sample (i.e., the crystallinity $w_{crys,25}$ at 25 °C). If $w_{crys,25}$ is unknown, it can be evaluated from eq 10 with an accuracy of 10% at worst.

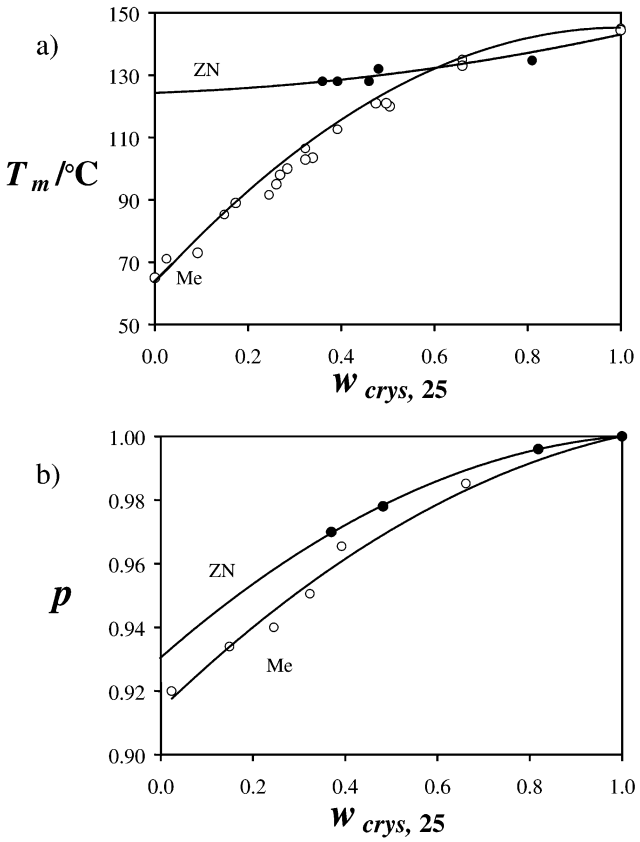

Figure 13. (a) Melting point of semicrystalline polyethylene T_m as a function of the experimental crystallinity $w_{crys,25}$ at 25 °C. The open circles (○) denote experimental melting points of samples made with metallocene (Me) catalysts, and the filled circles (●) denote those made with Ziegler−Natta (ZN) catalysts.[12,63] The continuous curves correspond to the correlations given by eqs 35 and 36. (b) Probability p that a crystallizable A unit in the polyethylene chain is followed by another A unit as a function of $w_{crys,25}$. The data (○ for Me, ● for ZN catalysts) correspond to the fitted p values obtained using eq 34 with experimental crystallinity versus temperature curves (cf. ref 14). The continuous curves correspond to the correlations given by eqs 37 and 38.

4. Solubility of Gases in Semicrystalline Polyethylene with the SAFT-VR/Flory Approach

It is clear from Figure 14 that polyethylene is semicrystalline below the melting point, which ranges from about 60 to 140 K depending on the sample. Above the melting point the polymer is in an amorphous fluid state and it is sufficient to consider just the vapor−liquid-phase equilibria in studies of the solubility of gases in polyethylene (cf. section 2.3). Below the melting point of the polymer, the phase behavior becomes more complex with equilibria between vapor, liquid (amorphous polymer), and solid (polymer crystallites) phases. The solubility of gases has been observed to be a linear function of crystallinity.[2,12] One can assume that the gas absorbs only in the amorphous regions of the polymer sample, and that the polymer molecules are either totally amorphous, or totally crystallized, i.e., there are no partially crystallized blocks along the chain. It can also be assumed that the presence of gas in the polymer sample does not affect the crystallinity and melting point (no cryoscopic effects), and that constraints due to swelling can be neglected. These effects may be quite important in certain cases, and should be included in a more complete treatment.

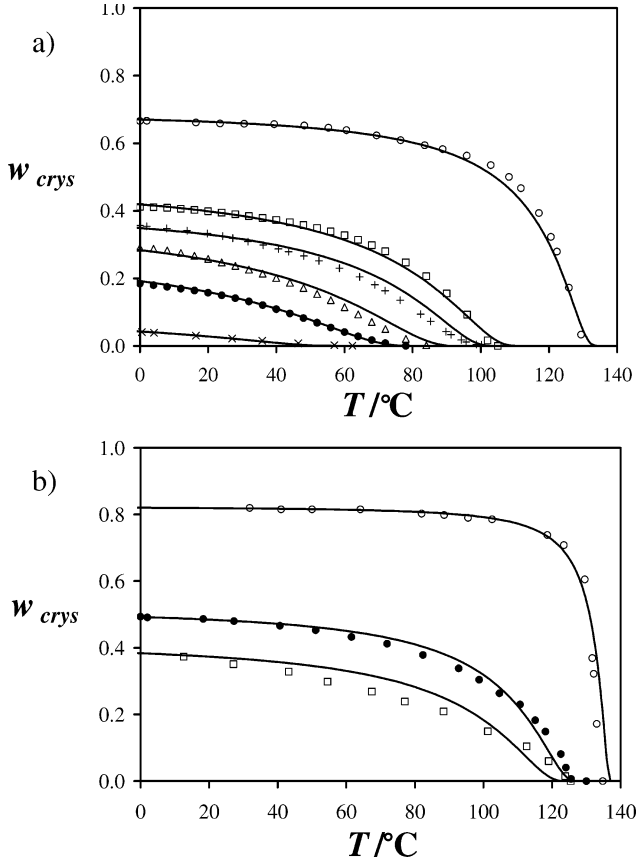

Figure 14. Crystallinity w_{crys} of polyethylene as a function of temperature T for samples produced with (a) metallocene and (b) Ziegler−Natta catalysts. The symbols represent the experimental data from references 12 and 63: (a) ○, EH1; □, EB2; +, EB4; △, EB5; ●, EB6; ×, EH6; (b) ○, 2757H; ●, EB1ZN; □, 2112L (see the corresponding papers for details about each sample). The continuous curves represent the predictions of the modified Flory approach eq 34 using the experimental value of $w_{crys,25}$, and the correlations 35−36 and 37−38 for T_m and p.

For semicrystalline polyethylene, the definition of solubility (eq 9) can be generalized to

$$Sol. = 100\frac{w_{gas}}{w_{PE}} = 100(1 - w_{crys}(T))\frac{w_{gas}^{(am)}}{w_{PE}^{(am)}}, \quad (39)$$

where w_{gas} and w_{PE} are the overall weight fractions of gas and polymer molecules in the sample, and $w_{gas}^{(am)}$ and $w_{PE}^{(am)}$ are the weight fractions of gas and polymer molecules in the amorphous phase at equilibrium. In our study $w_{gas}^{(am)}$ and $w_{PE}^{(am)}$ are determined with the SAFT-VR approach. The crystallinity of the pure polymer sample $w_{crys}(T)$ at the temperature of interest T, is estimated by using eq 34.

We compare our prediction of the absorption of α-olefins in semicrystalline HDPE and LDPE with the recent data of Moore et al.[2] The absorption curves for but-1-ene and hex-1-ene in HDPE and LDPE are displayed in Figures 15 and 16, respectively. The calculations are made using the SAFT-VR approach without the need for adjustable cross interaction parameters; i.e., with $k_{ij} = 0$. In reference 2 the experimental values for the crystallinity at 25 °C are reported as $w_{crys,25} = 0.702$ for the HDPE and $w_{crys,25} = 0.504$ for the LDPE. For the HDPE sample we use the correlations obtained for a ZN catalyst (eqs 35 and 37), and

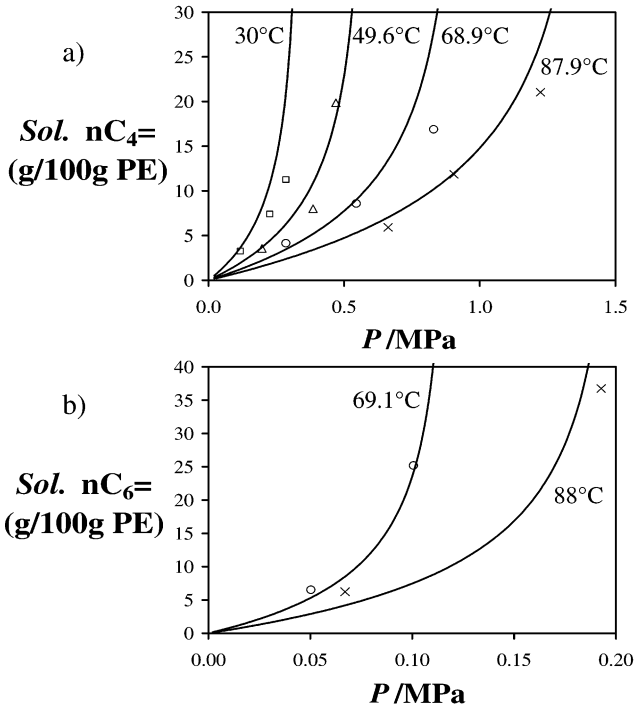

Figure 15. Solubility of (a) but-1-ene and (b) hex-1-ene in semicrystalline polyethylene (HDPE, MW = 11.49 kg mol^{-1}, $w_{crys,25}$ = 0.702). The SAFT-VR predictions of the vapor−liquid equilibria (continuous curves) are compared with experimental data[2] at different temperatures: (a) T = 30 °C (□), T = 49.6 °C (△), T = 68.9 °C (○), and T = 87.9 °C (×) for the but-1-ene system; and (b) T = 69.1 °C (○) and T = 88 °C (×) for the hex-1-ene system.

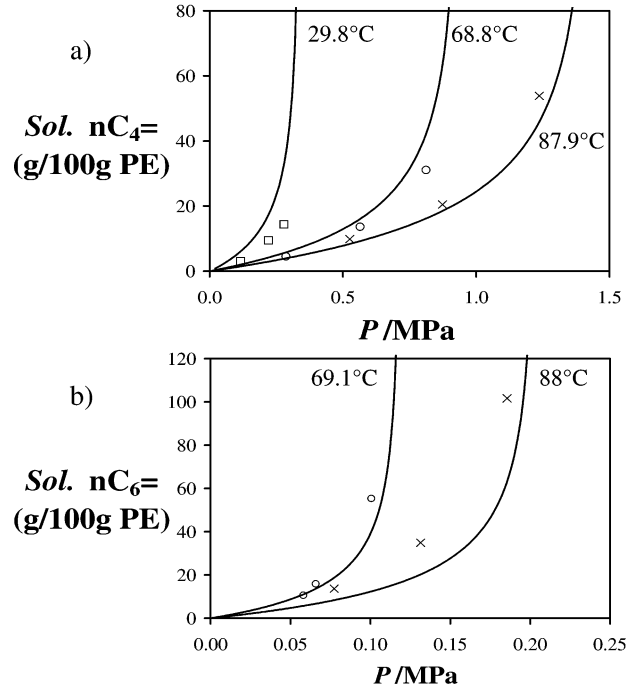

Figure 16. Solubility of (a) but-1-ene and (b) hex-1-ene in semicrystalline polyethylene (LDPE, MW = 22.01 kg mol^{-1}, $w_{crys,25}$ = 0.504). The SAFT-VR predictions of the vapor−liquid equilibria (continuous curves) are compared with experimental data[2] at different temperatures: (a) T = 29.8 °C (□), T = 68.8 °C (○), and T = 87.9 °C (×) for the but-1-ene system; and (b) T = 69.1 °C (○) and T = 88 °C (×) for the hex-1-ene system.

for the LDPE sample we use those for a Me catalyst (eqs 36 and 38). The temperature dependence of the

crystallinity for the HDPE and LDPE polymers is calculated with eq 34. The solubility of the given gas in the semicrystalline polymer is then predicted from eq 39 using the absorption curve obtained for amorphous polymer with the SAFT-VR equation of state. It is clear that a combination of the SAFT-VR (for the vapor−liquid equilibria) and scaled Flory (for the crystallinity) approaches provides a good predictive platform for the solubility of olefins in semicrystalline polyethylene over a wide range of temperatures. Though the overall description is good, the solubilities obtained from the approach appear to be overestimated at low temperature and high pressure. In this region of the phase diagram the crystallinity of HDPE is high and the absorption is limited by the constraints imposed on the swelling of the sample. At worst the theoretical predictions can deviate from the experimental data by up to a factor of 2, which indicates that the model should be improved. On the other hand, the solubility of hex-1-ene in LDPE is underestimated at high temperature and pressure (see Figure 16b). In this region the crystallinity of LDPE is low, and the effects due to constraints in swelling of the polymer are expected to be small. Here, the deviations may be due to cryoscopic effects: the presence of large amounts of gas in the sample decrease the melting point and the crystallinity of the polymer, and thus leads to an increase in the amount of amorphous polymer and an increase in the absorbed gas. One can see that constrained swelling and crysocopic effects shift the absorption curve in opposing ways; the dominance of one effect over the other depends on the temperature of the sample. We plan to take both effects into account in future work.

5. Conclusions

We have studied the fluid-phase behavior of mixtures of *n*-alkanes, α-olefins, and nitrogen with different polyethylene samples using the SAFT-VR approach. The intermolecular parameters for the pure components (other than the polymer) are refined by optimizing the description of the vapor pressure and saturated liquid density, while those for polyethylene are determined from simple extrapolations with molecular weight obtained for the *n*-alkanes. The theory provides a good description of the experimental data for the vapor−liquid equilibria, which in this case corresponds to the absorption of gases in amorphous polyethylene. The predictions obtained for the liquid−liquid equilibria (cloud curves) of solutions of polyethylene in *n*-alkane solvents are also satisfactory, though we have noted that the extent of liquid−liquid immiscibility is very sensitive to the parameters used to describe the pure polymer (due to the large number of segment−segment interactions involved). The overall agreement with experiment confirms the adequacy of the SAFT approach and the transferability of the parameters used to describe the various systems. The synergy of co-absorption of two gases in an amorphous sample of HDPE is also considered: hex-1-ene is found to enhance the solubility of but-1-ene quite dramatically, while the opposite is found in the presence of nitrogen. These findings can be understood in terms of the specific interactions between absorbed gases. The vapor−liquid equilibria for mixtures involving polyethylene at temperatures below the melting point of the pure polymer have been examined. In these cases, the polymer is semicrystalline, and the crystallinity (extent of solidification) of polyethylene has to be taken into account. An accurate approach which is based on the Flory theory of copolymer crystallization is developed to predict the crystallinity of arbitrary samples of polyethylene as a function of temperature. Quantitative predictions can be obtained with the scaled Flory theory using a single data point for the crystallinity of the sample at 25 °C. By applying the scaled Flory approach for the polymer crystallization together with the SAFT-VR description of the fluid-phase behavior, a good description of the absorption of α-olefins in polyethylene can be obtained by assuming that the gas molecules absorb only in the amorphous regions of the polyethylene sample. The additional problems involving cryoscopic effects and constraints due to swelling are currently being assessed. An alternative and novel use of our approach could be as an aid to the characterization of the degree of crystallinity of a given polymer sample for which gas phase absorption data are available; in view of the accuracy of the SAFT-VR predictions in describing gas absorption in amorphous polyethylene this novel approach could be particularly promising.

Acknowledgment

We express our thanks to Andrew Haslam, Jane Lipson, and Julia Higgins for useful discussions. P.P. thanks the Modelling Programme of BP Chemicals for funding a studentship, and A.G. thanks the Engineering and Physical Sciences Research Council (EPSRC) for the award of an Advanced Research Fellowship. We acknowledge further support from the EPSRC (GR/N03358, GR/N20317, GR/N35991, and GR/R09497), the Joint Research Equipment Initiative (JREI) for computer hardware (GR/M94427), and the Royal Society-Wolfson Foundation for the award of a refurbishment grant.

Literature Cited

(1) Hutchinson, R. A.; Ray, W. H. *J. Appl. Polym. Sci.* **1990**, *41*, 51.
(2) Moore, S. J.; Wanke, S. E. *Chem. Eng. Sci.* **2001**, *56*, 4121.
(3) Beret, S.; Muhle, M. E.; Villamil, I. A. *Chem. Eng. Prog.* **1977**, *73*, 44.
(4) Beret, S.; Hager, S. L. *J. Appl. Polym. Sci.* **1979**, *24*, 1787.
(5) Wertheim, M. S. *J. Stat. Phys.* **1984**, *35*, 19.
(6) Wertheim, M. S. *J. Stat. Phys.* **1984**, *35*, 35.
(7) Wertheim, M. S. *J. Stat. Phys.* **1986**, *42*, 459.
(8) Wertheim, M. S. *J. Stat. Phys.* **1986**, *42*, 477.
(9) Paricaud, P.; Galindo, A.; Jackson, G. *Mol. Phys.* **2003**, *101*, 2575.
(10) Paricaud, P.; Varga, S.; Jackson, G. *J. Chem. Phys.* **2003**, *118*, 8525.
(11) Michaels, A. S.; Parker, R. B. *J. Polym. Sci.* **1959**, *41*, 53.
(12) McKenna, T. F. *Eur. Polym. J.* **1998**, *34*, 1255.
(13) Nath, S. K.; de Pablo, J. J. *J. Phys. Chem. B* **1999**, *103*, 3539.
(14) Flaconneche, B.; Martin, J.; Klopffer, M. H. *Oil Gas Sci. Technol.* **2001**, *56* (3), 261.
(15) Lambert, S. M.; Song, Y.; Prausnitz, J. M. Equations of State for Polymer Systems. In *Equations of State for Fluids and Fluid Mixtures*; Sengers, J. V., Kayser, R. F., Peters, C. J., White, H. J., Jr., Eds.; Elsevier: Amsterdam, 2000; Vol. 2.
(16) Oishi, T.; Prausnitz, J. M. *Ind. Eng. Chem. Process Des. Dev.* **1978**, *17*, 333.
(17) Elbro, H. S.; Fredenslund, A.; Rasmussen, P. *Macromolecules* **1990**, *23*, 4707.
(18) Kontogeorgis, G. M.; Fredenslund, A.; Tassios, D. *Ind. Eng. Chem. Res.* **1993**, *32*, 362.
(19) Zhong, C. L.; Sato, Y.; Masuoka, H.; Chen, X. N. *Fluid Phase Equilib.* **1996**, *123*, 97.
(20) Chen, C. C. *Fluid Phase Equilib.* **1993**, *83*, 301.

(21) Wibawa, G.; Takishima, S.; Sato, Y.; Masuoka, H. *Fluid Phase Equilib.* **2002**, *202*, 367.
(22) Staverman, A. J.; Van Santen, J. H. *Recl. Trav. Chim. Pays Bas (Netherlands)* **1941**, *60*, 76. Staverman, A. J. *Recl. Trav. Chim. Pays Bas (Netherlands)* **1941**, *60*, 640.
(23) Flory, P. J. *J. Chem. Phys.* **1941**, *9*, 660.
(24) Huggins, M. L. *J. Chem. Phys.* **1941**, *9*, 440.
(25) Sanchez, I. C.; Lacombe, R. H. *J. Phys. Chem.* **1976**, *80*, 2352.
(26) Sanchez, I. C.; Lacombe, R. H. *Macromolecules* **1978**, *11*, 1145.
(27) Kirby, C. F.; McHugh, M. A. *Chem. Rev.* **1999**, *99*, 565.
(28) Bokis, C. P.; Orbey, H.; Chen, C. C. *Chem. Eng. Prog.* **1999**, *95*, 39.
(29) Xiong, Y.; Kiran, E. *J. Appl. Polym. Sci.* **1995**, *55*, 1805.
(30) Koak, N.; Heidemann, R. A. *Ind. Eng. Chem.* **1996**, *35*, 4301.
(31) Gauter, K.; Heidemann, R. A. *Fluid Phase Equilib.* **2001**, *183*, 87.
(32) Lipson, J. E. G. *Macromolecules* **1991**, *24*, 1334.
(33) Lipson, J. E. G. *J. Chem. Phys.* **1992**, *96*, 1418.
(34) Lipson, J. E. G.; Andrews, S. S. *J. Chem. Phys.* **1992**, *96*, 1426.
(35) Lipson, J. E. G.; Brazhnik, P. K. *J. Chem. Phys.* **1993**, *98*, 8178.
(36) Luettmer-Strathmann, J.; Lipson, J. E. G. *Fluid Phase Equilib.* **1988**, *151*, 649.
(37) Orbey, H.; Bokis, C. P.; Chen, C. C. *Ind. Eng. Chem. Res.* **1998**, *37*, 1567.
(38) Orbey, H.; Chen, C. C.; Bokis, C. P. *Fluid Phase Equilib.* **1998**, *145*, 169.
(39) Wertheim, M. S. *J. Chem. Phys.* **1987**, *87*, 7323.
(40) Chapman, W. G.; Jackson, G.; Gubbins, K. E. *Mol. Phys.* **1988**, *65*, 1057.
(41) Chapman, W. G.; Jackson, G.; Gubbins, K. E.; Radosz, M. *Fluid Phase Equil.* **1989**, *52*, 31.
(42) Chapman, W. G.; Jackson, G.; Gubbins, K. E.; Radosz, M. *Ind. Eng. Chem. Res.* **1990**, *29*, 1709.
(43) Huang, S. H.; Radosz, M. *Ind. Eng. Chem. Res.* **1990**, *29*, 2284.
(44) Huang, S. H.; Radosz, M. *Ind. Eng. Chem. Res.* **1991**, *30*, 1994.
(45) Müller, E. A.; Gubbins, K. E. *Ind. Eng. Chem. Res.* **1995**, *34*, 3662.
(46) Müller, E. A.; Gubbins, K. E. A Review of SAFT and Related Approaches. In *Equations of State for Fluids and Fluid Mixtures*; Sengers, J. V., Kayser, R. F., Peters, C. J., White, M. J., Jr., Eds.; Elsevier: Amsterdam, 2000.
(47) Blas, F. J.; Vega, L. F. *Mol. Phys.* **1997**, *92*, 135.
(48) Blas, F. J.; Vega, L. F. *Ind. Eng. Chem. Res.* **1998**, *37*, 660.
(49) Gil-Villegas, A.; Galindo, A.; Whitehead, P. J.; Mills, S. J.; Jackson, G.; Burgess, A. N. *J. Chem. Phys.* **1997**, *106*, 4168.
(50) Galindo, A.; Davies, L. A.; Gil-Villegas, A.; Jackson, G. *Mol. Phys.* **1998**, *93*, 241.
(51) Gross, J.; Sadowski, G. *Ind. Eng. Chem. Res.* **2001**, *40*, 1244.
(52) Gross, J.; Sadowski, G. *Ind. Eng. Chem. Res.* **2002**, *41*, 1084.
(53) Johnson, J. K.; Gubbins, K. E. *Mol. Phys.* **1992**, *77*, 1033.
(54) Blas, F. J.; Vega, L. F. *J. Chem. Phys.* **2001**, *115*, 4355.
(55) Johnson, J. K. *J. Chem. Phys.* **1996**, *104*, 1729.
(56) McCabe, C.; Galindo, A.; Garcıa-Lisbona, M. N.; Jackson, G. *Ind. Eng. Chem. Res.* **2001**, *40*, 3835.
(57) Mandelkern, L. *Crystallization of Polymers*; Series in Advanced Chemistry; McGraw-Hill: New York, 1964.
(58) Sharples, A. *Introduction to Polymer Crystallisation*; Edwards Arnold: London, 1966.
(59) Yoon, J. S.; Yoo, H. S.; Kang, K. S. *Eur. Polym. J.* **1996**, *32*, 1333.
(60) Marigo, A.; Marega, C.; Zannetti, R.; Sgarzi, P. *Eur. Polym. J.* **1998**, *34*, 597.
(61) Jordens, K.; Wilkes, G. L.; Janzen, J.; Rohlfing, D. C.; Welch, M. B. *Polymer* **2000**, *41*, 7175.
(62) Moreira, S. C.; Marques, M. D. V. *Eur. Polym. J.* **2001**, *37*, 2123.
(63) Starck, P.; Rajanen, K.; Loefgren, B. *Thermochim. Acta* **2003**, *395*, 169.
(64) Vega, C.; MacDowell, L. G. *J. Chem. Phys.* **2001**, *114*, 10411.
(65) McBride, C.; Vega, C. *J. Chem. Phys.* **2002**, *116*, 1757.
(66) Blas, F. J.; Galindo, A.; Vega, C. *Mol. Phys.* **2003**, *101*, 449.
(67) Vega, C.; Blas, F. J.; Galindo, A. *J. Chem. Phys.* **2002**, *116*, 7645.
(68) Vega, C.; McBride, C.; de Miguel, E.; Blas, F. J.; Galindo, A. *J. Chem. Phys.* **2003**, *118*, 10696.
(69) Flory, P. J. *Trans. Faraday Soc.* **1955**, *51*, 848.
(70) Sanchez, I. C.; Eby, R. K. *Macromolecules* **1975**, *8*, 638.
(71) Kim, M.-H.; Phillips, P. J.; Lin, J. S. *J. Polym. Sci., Part B: Polym. Phys.* **2000**, *38*, 154.
(72) Crist, B.; Howard, P. R. *Macromolecules* **1999**, *32*, 3057.
(73) Kubo, S.; Dole, M. *Macromolecules* **1973**, *6*, 774.
(74) Pan, C.; Radosz, M. *Ind. Eng. Chem. Res.* **1999**, *38*, 2842.
(75) Ghosh, A.; Chapman, W. G. *Ind. Eng. Chem. Res.* **2002**, *41*, 5529.
(76) Adidharma, H.; Radosz, M. *Ind. Eng. Chem. Res.* **2002**, *41*, 1774.
(77) Rogers, C. E.; Stannett, V.; Szwarc, M. *J. Phys. Chem.* **1959**, *63*, 1406.
(78) Michaels, A. S.; Hausslein, R. W. *J. Polym. Sci., Part C: Polym. Symp.* **1965**, *10*, 61.
(79) Li, N. N.; Long, R. B. *AIChE J.* **1969**, *15*, 73.
(80) Nath, S. K.; Banaszak, B. J.; de Pablo, J. J. *Macromolecules* **2001**, *34*, 7841.
(81) Barker, J. A.; Henderson, D. *J. Chem. Phys.* **1967**, *47*, 4714.
(82) Barker, J. A.; Henderson, D. *J. Chem. Phys.* **1967**, *47*, 2856.
(83) Barker, J. A.; Henderson, D. *Rev. Mod. Phys.* **1976**, *48*, 587.
(84) Boublık, T. *J. Chem. Phys.* **1970**, *53*, 471.
(85) Mansoori, G. A.; Carnahan, N. F.; Starling, K. E.; Leland, T. W. *J. Chem. Phys.* **1971**, *54*, 1523.
(86) Carnahan, N. F.; Starling, K. E. *J. Chem. Phys.* **1969**, *51*, 635.
(87) Hansen, J.-P.; McDonald, I. R. *Theory of Simple Liquids*; Academic Press: London, 1986.
(88) McCabe, C.; Jackson, G. *Phys. Chem. Chem. Phys.* **1999**, *1*, 2057.
(89) Smith, B. D.; Srivastava, R. *Thermodynamic Data for Pure Compounds*; Elsevier: Amsterdam, 1986.
(90) Press, W. H.; Teukolsky, S. A.; Vetterling, W. T.; Flannary Guevara, B. P. *Numerical Recipes in Fortran*; Cambridge University Press: London, 1986.
(91) Hino, T.; Prausnitz, J. M. *Fluid Phase Equilib.* **1997**, *138*, 105.
(92) Phoenix, A. V.; Heidemann, R. A. *Fluid Phase Equilib.* **1999**, *158*, 643.
(93) Kiran, E.; Xiong, Y.; Zhuang, W. H. *J. Supercritical Fluids* **1993**, *6*, 193.
(94) Xiong, Y.; Kiran, E. *Polymer* **1994**, *35*, 4408.
(95) Xiong, Y.; Kiran, E. *J. Appl. Polym. Sci.* **1994**, *53*, 1179.
(96) Surana, R. K.; Danner, R. P.; de Haan, A. B.; Beckers, N. *Fluid Phase Equilib.* **1997**, *139*, 361.
(97) Scott, R. L.; van Konynenburg, P. H. *Discuss. Faraday Soc.* **1970**, *49*, 87.
(98) Glaser, M.; Peters, C. J.; van der Kooi, H. J.; Lichtenthaler, R. N. *J. Chem. Thermodyn.* **1985**, *17*, 803.
(99) van der Kooi, H. J.; Flöter, E.; de Loos, T. W. *J. Chem. Thermodyn.* **1995**, *27*, 847.
(100) Flöter, E.; de Loos, T. W. *Int. J. Thermophys.* **1995**, *16*, 185.
(101) Flöter, E.; de Loos, T. W.; de Swaan Arons, J. *Fluid Phase Equilib.* **1997**, *127*, 129.
(102) Flöter, E.; Brumm, C.; de Loos, T. W.; de Swaan Arons, J. *J. Chem. Eng. Data* **1997**, *42*, 64.
(103) Flöter, E.; van der Pijl, P.; de Loos, T. W.; de Swaan Arons, J. *Fluid Phase Equilib.* **1997**, *134*, 1.
(104) Xiong, Y.; Kiran, E. *Polymer* **1999**, *36*, 4817.
(105) Luettmer-Strathmann, J.; Scoenhard, J. A.; Lipson, J. E. G. *Macromolecules* **1998**, *31*, 9231.
(106) Luettmer-Strathmann, J.; Lipson, J. E. G. *Macromolecules* **1999**, *32*, 1093.
(107) Flory, P. J.; Orwoll, R. A.; Vrij, J. A. *J. Am. Chem. Soc.* **1964**, *86*, 3515.
(108) Hamada, F.; Fujisawa, K.; Nakajima, A. *Polym. J.* **1973**, *4*, 316.
(109) Kodama, Y.; Swinton, F. L. *Brit. Polym. J.* **1978**, *10*, 191.
(110) Charlet, G.; Delmas, G. *Polymer* **1981**, *22*, 1181.
(111) de Loos, T. W.; de Graaf, L. J.; de Swaan Arons, J. *Fluid Phase Equilib.* **1996**, *117*, 40.

(112) Banaszak, B. J.; Faller, R.; de Pablo, J. J. *J. Chem. Phys.* **2004**, *120*, 11304.
(113) Garcıa-Sánchez, F.; Eliosa-Jiménez, G.; Silva-Oliver, G.; Vázquez-Román, R. *Fluid Phase Equilib.* **2004**, *217*, 241.
(114) Hao, W.; Elbro, H. S.; Alessi, P. *Polymer Solution Data Collection*; Vol. 14, part 1 of Chemistry Data Series; DECHEMA: Frankfurt, 1992.
(115) Sato, Y.; Fujiwara, K.; Takikawa, T.; Sumarno; Takishima, S.; Masuoka, H. *Fluid Phase Equilib.* **1999**, *162*, 261.
(116) Laugier, S.; Richon, D. *J. Chem. Eng. Data* **1996**, *41*, 282.
(117) Yiagopoulos, A.; Yiannoulakis, H.; Dimos, V.; Kiparissides, C. *Chem. Eng. Sci.* **2001**, *56*, 3979.
(118) Widom, B. *J. Chem. Phys.* **1963**, *39*, 2808. Widom, B. *J. Stat. Phys.* **1978**, *19*, 563.

Received for review May 14, 2004
Revised manuscript received July 19, 2004
Accepted July 26, 2004

IE049592A